Neurobiology of Disease 164 (2022) 105628

Contents lists available at ScienceDirect

Neurobiology of Disease

journal homepage: www.elsevier.com/locate/ynbdi

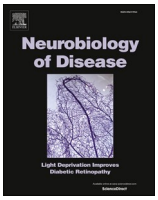

Intravitreal gene therapy restores the autophagy-lysosomal pathway and attenuates retinal degeneration in cathepsin D-deficient mice

Junling Liu [a], Mahmoud Bassal [a], Stefanie Schlichting [a], Ingke Braren [b], Alessandro Di Spiezio [c], Paul Saftig [c], Udo Bartsch [a,*]

[a] Department of Ophthalmology, Experimental Ophthalmology, University Medical Center Hamburg-Eppendorf, 20246 Hamburg, Germany
[b] Vector Facility, University Medical Center Hamburg-Eppendorf, 20246 Hamburg, Germany
[c] Institute of Biochemistry, Christian-Albrechts-University Kiel, 24118 Kiel, Germany

ARTICLE INFO

Keywords:
Autophagy
Cathepsin D
CLN10 disease
Enzyme replacement therapy
Gene therapy
Lysosome
Neural stem cells
Neuronal ceroid lipofuscinosis
Retinal degeneration

ABSTRACT

Loss of vision due to progressive retinal degeneration is a hallmark of neuronal ceroid lipofuscinoses (NCL), a group of fatal neurodegenerative lysosomal storage diseases. Enzyme substitution therapies represent promising treatment options for NCLs caused by dysfunctions of soluble lysosomal enzymes. Here, we compared the efficacy of a cell-based enzyme substitution strategy and a gene therapy approach to attenuate the retinal pathology in cathepsin D- (CTSD) deficient mice, an animal model of CLN10 disease. Levels of enzymatically active CTSD in mutant retinas were significantly higher after an adeno-associated virus vector-mediated CTSD transfer to retinal glial cells and retinal pigment epithelial cells than after intravitreal transplantations of a CTSD overexpressing clonal neural stem cell line. In line with this finding, the gene therapy treatment restored the disrupted autophagy-lysosomal pathway more effectively than the cell-based approach, as indicated by a complete clearance of storage, significant attenuation of lysosomal hypertrophy, and normalized levels of the autophagy marker sequestosome 1/p62 and microtubule-associated protein 1 light chain 3-II. While the cell-based treatment did not prevent the rapidly progressing loss of various retinal cell types, the gene therapy approach markedly attenuated retinal degeneration as demonstrated by a pronounced rescue of photoreceptor cells and rod bipolar cells.

1. Introduction

Neuronal ceroid lipofuscinosis (NCL) comprises a genetically and clinically heterogeneous group of neurodegenerative lysosomal storage diseases (Johnson et al., 2019; Kohlschutter et al., 2019; Mole et al., 2019). The disease is caused by mutations in 13 different genes (CLN1 to CLN8, CLN10 to CLN14) encoding proteins with diverse and partly unknown functions and different intracellular locations, albeit most reside in lysosomes (Carcel-Trullols et al., 2015; Kohlschutter et al., 2019; Kollmann et al., 2013; Mukherjee et al., 2019). Clinical symptoms of NCL patients usually start in childhood or youth, are neuronal in origin, and typically include progressive cognitive decline, motor deterioration, seizures, vision loss and premature death. Intracellular accumulation of autofluorescent storage material and progressive neurodegeneration are hallmarks of all NCL forms (Johnson et al., 2019; Kohlschutter et al., 2019; Mole et al., 2019; Radke et al., 2015; Schulz et al., 2013). Impaired macroautophagy (hereafter referred to as autophagy), a catabolic process by which cytoplasmic cargo is sequestered and delivered to

Abbreviations: AAV, adeno-associated virus; BSD, blasticidin; CTSD, cathepsin D; CTSZ, cathepsin X/Z/P; CD68, cluster of differentiation 68; CTSD-NSCs, CTSD overexpressing neural stem cells; GAPDH, glyceraldehyde 3-phosphate dehydrogenase; GFAP, glial fibrillary acidic protein; GFP, green fluorescent protein; HEK, human embryonic kidney; IBA1, ionized calcium-binding adapter molecule 1; iCTSD, intermediate CTSD; IRES, internal ribosome entry site; ko, knockout; ko-NSCs, knockout neural stem cells; LAMP1, lysosomal-associated membrane protein 1; LAMP2, lysosomal-associated membrane protein 2; LAP, LC3-associated phagocytosis; MAP2, microtubule-associated protein 2; mCTSD, mature cathepsin D; MAP1LC3-I/II, microtubule-associated protein 1 light chain 3-I/II; NCL, neuronal ceroid lipofuscinosis; NSCs, neural stem cells; PCR, polymerase chain reaction; POS, photoreceptor outer segments; PPT1, palmitoyl-protein thioesterase 1; pCTSD, pro-CTSD; PKCα, protein kinase C-alpha; rhCTSD, recombinant human CTSD; RPE, retinal pigment epithelial; sc, self-complementary; SCGN, secretagogin; SCMAS, subunit c of mitochondrial ATP synthase; SQSTM1/p62, sequestosome 1/p62; TPP1, tripeptidyl-peptidase 1; wt, wild-type; wt-NSCs, wild-type neural stem cells.

* Corresponding author at: Department of Ophthalmology, University Medical Center Hamburg-Eppendorf, Martinistr. 52, 20246 Hamburg, Germany.
E-mail address: ubartsch@uke.de (U. Bartsch).

https://doi.org/10.1016/j.nbd.2022.105628
Received 18 October 2021; Received in revised form 7 January 2022; Accepted 10 January 2022
Available online 13 January 2022

lysosomes for degradation by hydrolases, has been recognized as a common disease mechanism of several lysosomal storage diseases, including different NCLs (Adams et al., 2019; Brandenstein et al., 2016; Cao et al., 2006; Koike et al., 2005; Leinonen et al., 2017; Thelen et al., 2012; von Eisenhart-Rothe et al., 2018; Wavre-Shapton et al., 2015).

CLN10 disease is caused by mutations in the gene encoding cathepsin D (CTSD) (Siintola et al., 2006; Steinfeld et al., 2006), a ubiquitously expressed lysosomal aspartic endoprotease. Similar to all other cathepsins, CTSD is synthesized as a pre-pro-enzyme. After co-translational removal of the signal peptide, the zymogen is targeted mainly *via* a mannose-6-phosphate (M6P)-dependent pathway to the endolysosomal compartment where the pro-peptide is removed in late endosomes to generate an active intermediate single-chain molecule (iCTSD). Further proteolytic processing into the mature double-chain form consisting of an amino-terminal light chain and a carboxy-terminal heavy chain (mCTSD) occurs in the lysosome (Laurent-Matha et al., 2006; Zaidi et al., 2008). The protease is engaged in the degradation of macromolecules and organelles, and additionally performs various other functions such as proteolytic activation of growth factors, hormones and enzyme precursors, and regulation of apoptosis (Benes et al., 2008; Mijanovic et al., 2021; Vidoni et al., 2016). Loss-of-function mutations in the gene encoding CTSD result in accumulation of storage material and disruption of the autophagic flux (Bassal et al., 2021; Koike et al., 2005; Marques et al., 2020).

Complete loss and partial loss of CTSD enzymatic activity cause congenital and infantile, juvenile or adult CLN10 disease, respectively. Congenital CLN10 disease is the most severe NCL form, and affected patients present with respiratory failure, rigidity, seizures, microcephaly, and intrauterine or early postnatal death (Fritchie et al., 2009; Meyer et al., 2015; Siintola et al., 2006; Varvagiannis et al., 2018). Patients with late-onset CLN10 disease present with ataxia, progressive cognitive decline, motor deterioration and progressive vision loss due to retinal degeneration (Doccini et al., 2016; Hersheson et al., 2014; Regensburger et al., 2020; Steinfeld et al., 2006; Thottath et al., 2019). *Ctsd* knockout (ko) mice faithfully recapitulate key features of human CLN10 disease, including accumulation of storage material, brain atrophy and premature death around postnatal day (P) 26 (Koike et al., 2000; Saftig et al., 1995). The mutant mouse also shows an early-onset and rapidly progressing retinal dystrophy (Bassal et al., 2021; Koike et al., 2003). We have recently performed a detailed analysis of the time course of the retinal dystrophy in the mutant mice (Bassal et al., 2021). Pathological features include an early-onset accumulation of storage material, reactive astrogliosis and microgliosis, lysosomal hypertrophy and an impaired autophagic flux as indicated by a progressive accumulation of the autophagy cargo receptor sequestosome 1/p62 (SQSTM1/p62). Degeneration of photoreceptor cells started early during the course of the disease and was followed by a pronounced loss of essentially all retinal cell types, resulting in a severely atrophied retina at the end stage of the disease (Bassal et al., 2021).

Enzyme substitution therapies represent promising treatment options for NCLs caused by dysfunctions of lysosomal enzymes. Preclinical work has demonstrated a marked attenuation of disease progression in CLN1, CLN2 and CLN10 animal models after administration of functional variants of the defective or missing enzymes to the brain (Johnson et al., 2019; Kohlschutter et al., 2019; Mole et al., 2019; Specchio et al., 2021). Notably, recent clinical trials have also demonstrated a slower decline of neurological symptoms in CLN2 patients treated with repeated intracerebroventricular injections of recombinant tripeptidyl-peptidase 1 (TPP1) or intraparenchymal injections of an adeno-associated virus (AAV) vector encoding TPP1, the lysosomal enzyme affected in this disease (Schaefers et al., 2021; Schulz et al., 2018; Sondhi et al., 2020). Different to the brain, however, only a few studies have evaluated the impact of enzyme substitution therapies on the progression of retinal degeneration and vision loss in these NCLs.

In the present study, we have evaluated the outcome of a sustained intraocular administration of CTSD, achieved through either an AAV vector-mediated *Ctsd* gene transfer to the mutant retina or intravitreal injections of a CTSD overexpressing neural stem cell (NSC) line. The gene therapy approach resulted in significantly higher levels of enzymatically active CTSD in mutant retinas and restored the disrupted autophagy-lysosomal pathway more effectively than the cell-based approach. In line with these findings, attenuation of retinal degeneration was only observed with the gene therapy treatment.

2. Results

2.1. Expression of CTSD in undifferentiated and differentiated neural stem cells and cellular uptake of CTSD in vitro

To analyze the expression of CTSD in undifferentiated and differentiated NSCs *in vitro*, immunocytochemical analyses were performed on *Ctsd* ko NSCs (ko-NSCs), wild-type NSCs (wt-NSCs), CTSD overexpressing NSCs (CTSD-NSCs), and astrocytes and neurons derived from these stem cells (Fig. 1A). ko-NSCs and glial fibrillary acidic protein (GFAP)-positive astrocytes and microtubule-associated protein 2 (MAP2)-positive neurons derived from ko-NSCs (ko-astrocytes and ko-neurons, respectively) expressed the reporter gene Venus but no detectable levels of CTSD (Fig. 1A), as expected. wt-NSCs, wt-astrocytes and wt-neurons expressed the reporter protein tdTomato and were CTSD-positive (Fig. 1A). tdTomato-positive CTSD-NSCs and CTSD-overexpressing astrocytes and neurons (CTSD-astrocytes and CTSD-neurons, respectively) expressed significantly higher levels of CTSD than the corresponding wt cell types (Fig. 1A).

Cellular uptake of CTSD *in vitro* was analyzed in co-cultures consisting of tdTomato-positive CTSD-astrocytes and ko-astrocytes (Fig. S1). While cells in pure ko-astrocyte cultures were CTSD negative, CTSD was detectable in ko-astrocytes co-cultured with CTSD-astrocytes where the enzyme co-localized with the lysosomal marker lysosomal-associated membrane protein 1 (LAMP1) or lysosomal-associated membrane protein 2 (LAMP2; Fig. S1). In addition, levels of LAMP1 and LAMP2 in ko-astrocytes co-cultured with CTSD-astrocytes were significantly decreased when compared with pure ko-astrocyte cultures (Fig. S1). To further confirm cellular uptake of CTSD *in vitro*, ko-astrocytes were cultured for 7 days in conditioned medium from either ko-astrocytes or CTSD-astrocytes. Immunocytochemical analyses revealed that ko-astrocytes cultured in conditioned medium from ko-astrocytes showed elevated LAMP1 and LAMP2 signals, both in number and in size, when compared to ko-astrocytes cultured in conditioned medium from CTSD-astrocytes (Fig. 1B). Co-localization of CTSD and LAMP1 or LAMP2 in ko-astrocytes cultured in conditioned medium from CTSD-astrocytes (Fig. 1B) suggested uptake of CTSD and transport into LAMP1- or LAMP2-positive endolysosomes.

Western blot analyses demonstrated the presence of pro-CTSD (pCTSD) in culture supernatants from CTSD-NSCs and CTSD-astrocytes, and at lower level in supernatants from wt-NSCs and wt-astrocytes (Fig. 1C), indicating release of CTSD from these cells. No signal was detected in supernatants from ko-NSCs and ko-astrocytes. Western blot analyses of cell lysates (Fig. 1C) revealed that CTSD-NSCs, wt-NSCs and astrocytes derived from these stem cells contained pCTSD, intermediate-CTSD (iCTSD) and mature-CTSD (mCTSD), with iCTSD being the predominant form. Intensities of CTSD signals in CTSD-NSCs and CTSD-astrocytes were markedly higher than in wt-NSCs and wt-astrocytes, respectively (Fig. 1C). No CTSD was detected in ko-NSCs and ko-astrocytes. Importantly, iCTSD was detected in ko-astrocytes cultured in conditioned medium from CTSD astrocytes, indicating uptake and processing of pCTSD by ko-astrocytes. In contrast, CTSD was not detectable in ko-astrocytes cultured in conditioned medium from ko-astrocytes (Fig. 1C). Analyses of CTSD enzymatic activity in cell lysates from NSC cultures (Fig. 1D) revealed a 3.4-fold ± 0.05 (mean $\pm$ SEM) higher activity in CTSD-NSCs than in wt-NSCs.

To analyze CTSD uptake by retinal cell types, we maintained primary retinal cell cultures from *Ctsd* ko mice in conditioned media from either

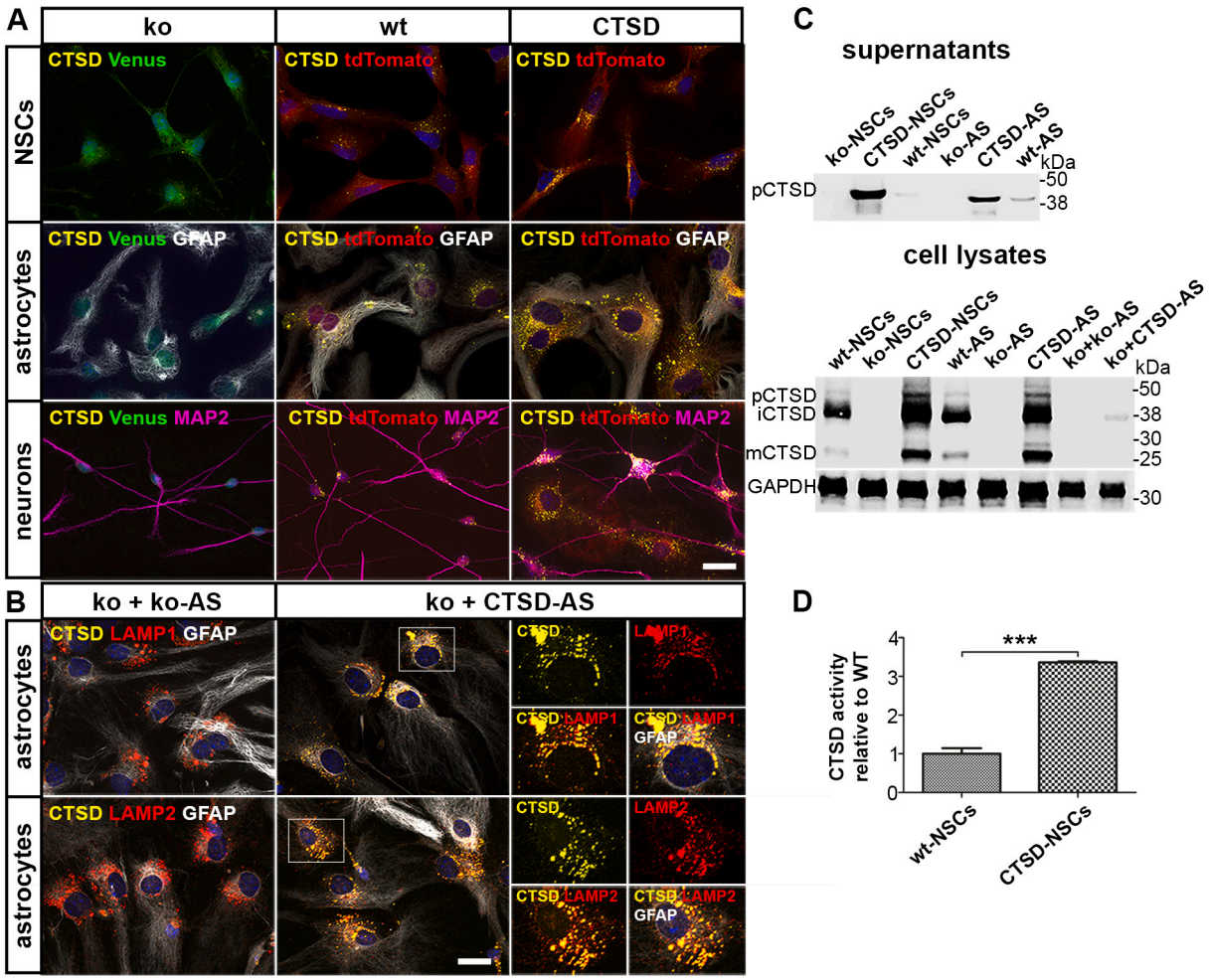

Fig. 1. Expression and enzymatic activity of CTSD in undifferentiated and differentiated NSCs and uptake of CTSD by NSC-derived astrocytes.
(A) CTSD immunostainings of undifferentiated clonal NSC lines, NSC-derived GFAP-positive astrocytes and NSC-derived MAP2-positive neurons. (B) Co-localization of CTSD and LAMP1 or CTSD and LAMP2 in ko-astrocytes cultured in the presence of conditioned medium from either ko-astrocytes (ko + ko-AS) or CTSD-astrocytes (ko + CTSD-AS). The boxed areas are shown at higher magnification in the right hand panels. (C) CTSD immunoblots of supernatants or cell lysates from different NSC cultures and NSC-derived astrocytes. (D) CTSD enzymatic activity in wt-NSCs and CTSD-NSCs. Each bar represents the mean value (±SEM) of 4 independent cultures. ***, $p < 0.001$, unpaired Student's *t*-test. AS, astrocytes; CTSD, cathepsin D; NSCs, neural stem cells; GAPDH, glyceraldehyde-3-phosphate dehydrogenase; GFAP, glial fibrillary acidic protein; iCTSD, intermediate-CTSD; ko, knockout; ko + ko-AS, *Ctsd* ko astrocytes maintained in conditioned medium from *Ctsd* ko-astrocytes; ko + CTSD-AS, *Ctsd* ko astrocytes maintained in conditioned medium from CTSD-astrocytes. LAMP1, lysosomal-associated membrane protein 1; LAMP2, lysosomal-associated membrane protein 2; MAP2, microtubule-associated protein 2; mCTSD, mature-CTSD; wt, wild-type; pCTSD, pro-CTSD. Scale bars, 20 μm.

ko-astrocytes or CTSD-astrocytes (Fig. 2). CTSD labeling was observed in different retinal cell types maintained in conditioned medium from CTSD-astrocytes, including arrestin-positive cone photoreceptor cells, rhodopsin-positive rod photoreceptor cells, protein kinase C alpha (PKCα)-positive rod bipolar cells, β-tubulin III positive neurons and GFAP-positive astrocytes/Müller cells. Retinal cells maintained in conditioned media from ko-astrocytes were CTSD-negative (Fig. 2).

2.2. AAVshH10 transduces retinal pigment epithelial cells and Müller cells

To investigate the tropism of the AAVshH10 serotype in the murine retina, we intravitreally injected scAAVshH10-CMV-GFP (scAAVshH10-GFP; 1 μl, 2.5×10^{12} vg/μl) into *Ctsd* wt mice at P5. At P22, we observed robust expression of green fluorescent protein (GFP) throughout the retina (Fig. S2A). Co-localization of GFP with glutamine-synthetase (GS) or GFAP demonstrated efficient transduction of Müller glia. GFP expression was also found in retinal pigment epithelial (RPE) cells (Fig. S2A). To investigate the time course of CTSD expression, 1 μl of scAAVshH10-GFP or scAAVshH10-CMV-CTSD (scAAVshH10-CTSD; 2.5×10^{12} vg/μl each) was intravitreally injected into P5 *Ctsd* ko mice, and retinas were analyzed 4 days later. At this time point, transgene expression was detectable in localized areas of the treated retinas. Usually, GFP or CTSD expression was more pronounced in central retina regions than in peripheral retina regions (Fig. S2B).

2.3. Correction of the biochemical phenotype of Ctsd ko retinas after intravitreal injections of NSCs or AAV particles

Ctsd ko retinas display an early onset accumulation of storage material and a marked dysregulation of various lysosomal proteins (Bassal et al., 2021). After intravitreal transplantations of CTSD-NSCs at P7 and analyses of retinas at P22, CTSD was detectable in all layers of the treated retinas, while retinas of the contralateral eyes injected with ko-NSCs were CTSD-negative (Fig. 3). Uptake of CTSD by retinal cells resulted in partial correction of various pathological markers. For instance, levels of saposin D and subunit c of mitochondrial ATP synthase (SCMAS) were markedly reduced in mutant retinas with grafted

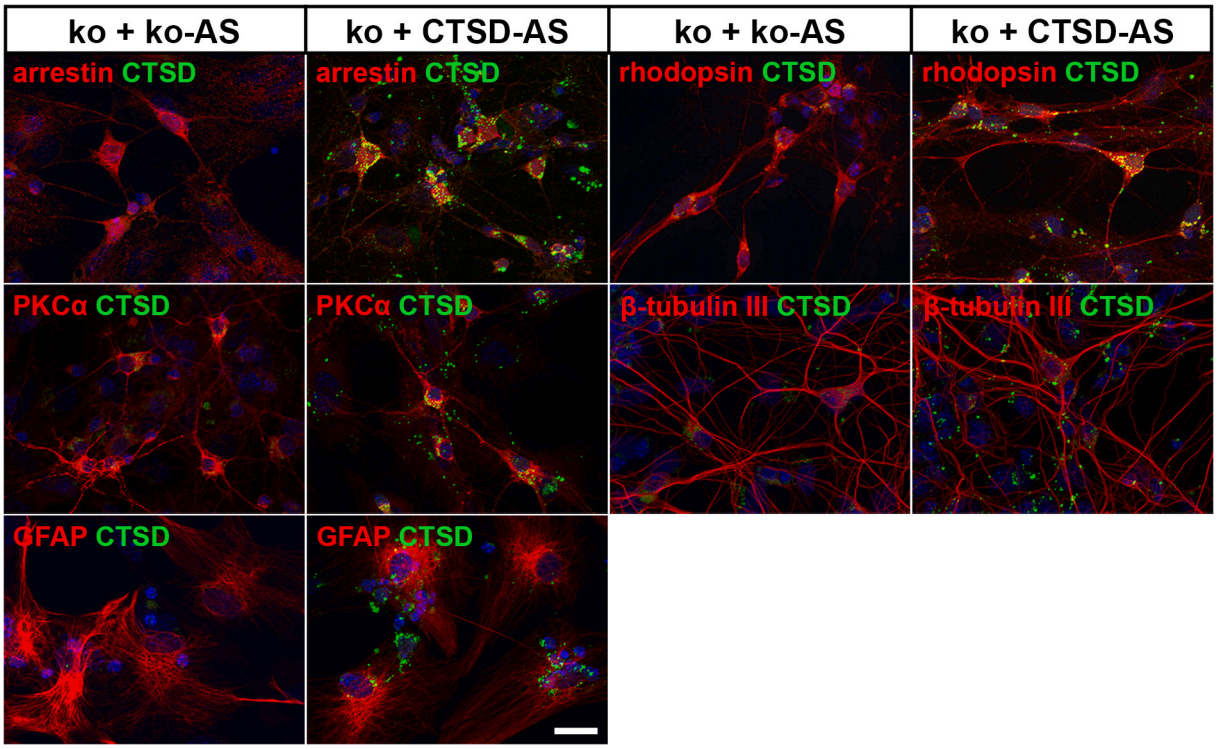

Fig. 2. Uptake of CTSD by different CTSD-deficient retinal cell types *in vitro*.
Double-immunostainings of primary retinal cell cultures maintained in conditioned medium from ko-astrocytes (ko + ko-AS) or CTSD-astrocytes (ko + CTSD-AS) with antibodies to CTSD and either cone-arrestin, rhodopsin, PKCα, β-tubulin III or GFAP. CTSD, cathepsin D; GFAP, glial fibrillary acidic protein; ko, knockout; ko + ko-AS, *Ctsd* ko primary retinal cell cultures maintained in conditioned medium from ko-astrocytes; ko + CTSD-AS, *Ctsd* ko primary retinal cell cultures maintained in conditioned medium from CTSD-astrocytes; PKC*α*, protein kinase C-alpha. Scale bar, 20 μm.

CTSD-NSCs when compared to control retinas with grafted ko-NSCs (Fig. 3). In addition, levels of the lysosomal proteins LAMP1, LAMP2 and cathepsin X/Z/P (CTSZ) in the neuroretina of CTSD-NSC-treated *Ctsd* ko mice were decreased when compared to control retinas (Fig. 3), indicating partial correction of the lysosomal hypertrophy. Levels of LAMP1 and LAMP2 in the RPE of treated eyes were, however, similar to those found in control eyes (Fig. S3). SQSTM1/p62-positive punctae were detectable in various retinal nerve cell types of untreated *Ctsd* ko retinas, including cone photoreceptor cells, rod bipolar cells and cone bipolar cells (Fig. S4). Of note, the density of p62 bodies was markedly decreased in retinas with grafted CTSD-NSCs when compared to control retinas (Fig. 3), indicating attenuation of autophagic dysfunction.

Intravitreal injections of scAAVshH10-CTSD into mutant mice resulted in significantly higher levels of CTSD than intravitreal transplantations of CTSD-NSCs, both in the neuroretina and the RPE (Fig. 4). Higher CTSD levels correlated with a more pronounced correction of the biochemical phenotype. For instance, the amount of storage material in scAAVshH10-CTSD-treated retinas was markedly more reduced than in NSC-treated retinas, as indicated by immunostainings with antibodies to saposin D and SCMAS (compare Figs. 4 and 3). Additionally, expression levels of LAMP1, LAMP2 and CTSZ in the neuroretina were clearly more reduced after injections of scAAVshH10-CTSD than after transplantations of CTSD-NSCs (compare Figs. 4 and 3). Levels of LAMP2, but not LAMP1, were also markedly decreased in the RPE of treated eyes (Fig. S3). Furthermore, and different to control retinas or CTSD-NSC-treated retinas, scAAVshH10-CTSD-treated retinas were completely devoid of SQSTM1/p62-positive punctae (Fig. 4) suggesting a normal autophagic flow. In summary, immunohistochemical analyses revealed that reduction of storage material, attenuation of lysosomal hypertrophy and amelioration of autophagic dysfunction was more pronounced in AAV-treated than in NSC-treated *Ctsd* ko retinas.

To identify the retinal cell types which took up the protease, we performed double immunostainings of scAAVshH10-CTSD injected retinas with antibodies to CTSD and various cell type-specific antigens (Fig. S5). Analyses revealed the presence of the enzyme in arrestin-, m opsin- or s opsin-positive cones, PKCα-positive rod bipolar cells, secretagogin (SCGN)-positive cone bipolar cells, ionized calcium-binding adapter molecule 1 (IBA1)-positive microglia and GFAP-positive astrocytes/Müller cells, indicating that a fraction of CTSD expressed by retinal glial cells and RPE cells was released into the extracellular space from where it was taken up by multiple retinal cell types (Fig. S5).

Western blot analysis revealed pCTSD, iCTSD and mCTSD in wt retinas and *Ctsd* ko retinas treated with CTSD-NSCs or scAAVshH10-CTSD, with iCTSD and mCTSD being the predominant forms (Fig. 5A). Untreated *Ctsd* ko retinas and mutant retinas treated with ko-NSCs or scAAVshH10-GFP were completely devoid of CTSD, as expected (Fig. 5A). Quantitative analyses (Fig. 5B) revealed that the amount of iCTSD and mCTSD in CTSD-NSC-treated retinas accounted to 31% and 40%, respectively of that found in wt retinas. In comparison, levels of iCTSD and mCTSD were markedly increased in scAAVshH10-CTSD-treated retinas by a factor of 5.22 ± 0.64 (mean ± SEM) and 7.27 ± 1.13, respectively when compared to wt retinas (Fig. 5B). Saposin D was significantly decreased in eyes with injected CTSD-NSCs or scAAVshH10-CTSD when compared to the contralateral control eyes (Fig. 5A, B). Of note, the amount of saposin D in AAV-treated *Ctsd* ko retinas was not significantly different from that found in untreated wt retinas (Fig. 5B). SCMAS was also significantly decreased in CTSD-NSC- and scAAVshH10-CTSD-treated retinas (Fig. 5A, B) to levels found in wt retinas. Furthermore, LAMP1 and LAMP2 were markedly decreased in eyes with injected scAAVshH10-CTSD or CTSD-NSCs when compared to control retinas (Fig. 5A, B), but were still significantly higher than in untreated wt retinas (Fig. 5B). Lysosomal dysfunction as indicated by the accumulation of SQSTM1/p62 and accumulation of

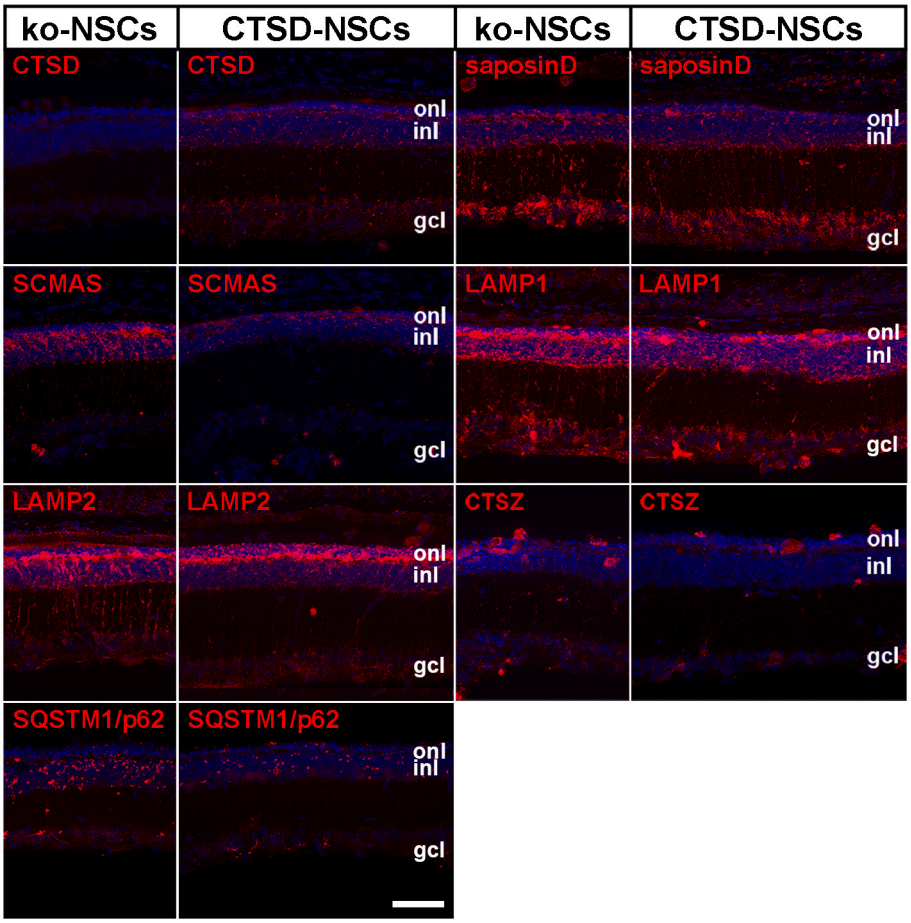

Fig. 3. Impact of intravitreally grafted CTSD-NSCs on the biochemical phenotype of *Ctsd* ko retinas. Immunohistochemical analyses of retinas from P22 *Ctsd* ko mice with grafted CTSD-NSCs and contralateral control eyes with grafted ko-NSCs with antibodies to CTSD, saposin D, SCMAS, LAMP1, LAMP2, CTSZ and SQSTM1/P62. CTSD, cathepsin D; CTSZ, cathepsin X/Z/P; gcl, ganglion cell layer; inl, inner nuclear layer; ko, knockout; LAMP1, lysosomal-associated membrane protein 1; LAMP2, lysosomal-associated membrane protein 2; NSCs, neural stem cells; onl, outer nuclear layer; SCMAS, subunit c of mitochondrial ATP synthase; SQSTM1/p62, sequestosome 1/p62. Scale bar, 50 μm.

autophagosomes as indicated by elevated levels of microtubule-associated protein 1 light chain 3-II (LC3-II) were not significantly attenuated after injections of CTSD-NSCs. However, in retinas treated with scAAVshH10-CTSD, SQSTM1/p62 and LC3-II were significantly decreased to levels found in untreated wt retinas (Fig. 5A, B). Finally, levels of saposin D, SCMAS, LAMP1, LAMP2, SQSTM1/p62 and LC3-II in wt retinas treated with CTSD-NSCs were not significantly different from those in wt retinas with grafted ko-NSCs (Fig. 5A, B), demonstrating that the sustained administration of CTSD had no impact on the expression levels of these proteins in healthy retinas.

CTSD enzymatic activity in *Ctsd* ko retinas treated with CTSD-NSCs accounted for ~44% of the enzymatic activity measured in untreated wt retinas ($p < 0.05$, one-way ANOVA, Fig. 5C). In comparison, levels of CTSD activity in scAAVshH10-CTSD treated *Ctsd* ko retinas were not significantly different from those found in untreated wt retinas, accounting for ~89% of the value in healthy retinas ($p > 0.05$, one-way ANOVA, Fig. 5C).

2.4. Attenuation of neuroinflammation in treated Ctsd ko retinas

Immunohistochemical analyses of retinas injected with CTSD-NSCs or scAAVshH10-CTSD showed significant attenuation of reactive microgliosis and astrogliosis when compared to the contralateral control eyes. Qualitative analyses of retina sections suggested a decreased density of IBA1-positive microglia in mutant retinas with transplanted CTSD-NSCs when compared to retinas with transplanted ko-NSCs (Fig. 6A, Fig. S6). However, attenuation of reactive microgliosis was markedly more pronounced in retinas treated with scAAVshH10-CTSD. Compared to control retinas, IBA1-positive microglia cells in scAAVshH10-CTSD-treated retinas had a more ramified morphology and were almost absent from the subretinal space and outer nuclear layer (Fig. 6A, Fig. S6). Similarly, cluster of differentiation 68 (CD68)-positive microglia/macrophages were markedly decreased in number in CTSD-NSCs-treated retinas, but the effect was significantly more pronounced in scAAVshH10-CTSD injected retinas (Fig. 6A). Quantitative analyses showed that the density of CD68-positive cells was reduced by 25.6% in CTSD-NSCs-treated retinas, as opposed to 67.4% in scAAVshH10-CTSD injected retinas when compared to the corresponding control retinas ($p < 0.05$ and $p < 0.001$, respectively, paired *t*-test; Fig. 6B). Furthermore, and similar to IBA1-positive cells, CD68-positive microglia/macrophages were almost completely absent from the subretinal space of AAV-treated retinas (Fig. 6A).

In addition, the high expression levels of GFAP in astrocytes and Müller cells observed in control retinas were significantly decreased in eyes with injected CTSD-NSCs or scAAVshH10-CTSD (Fig. 6).

2.5. CTSD substitution with CTSD-NSCs did not attenuate retinal degeneration in Ctsd ko mice

We next quantified the densities of different retinal cell types in CTSD-NSC treated retinas at P22 to evaluate the impact of the treatment on retina structure (Fig. 7). Analyses revealed that the number of rows of photoreceptor nuclei in CTSD-NSC-treated retinas (1.75 ± 0.39; mean ± SEM) was similar to that found in the contralateral control retinas (1.77 ± 0.23; $p > 0.05$, paired *t*-test; Fig. 7B). Furthermore, immunohistochemical analyses revealed the presence of only a few m + s opsin- (1.71 ± 0.72/250 μm retina length; Fig. 7A, B) or arrestin- (0.10 ± 0.07/250 μm; Fig. 7A, B) positive cones in treated retinas, not significantly different from the number of m + s opsin- (0.40 ± 0.17/250 μm; Fig. 7A, B) or arrestin- (0.02 ± 0.02/250 μm; Fig. 7A, B) positive cones found in

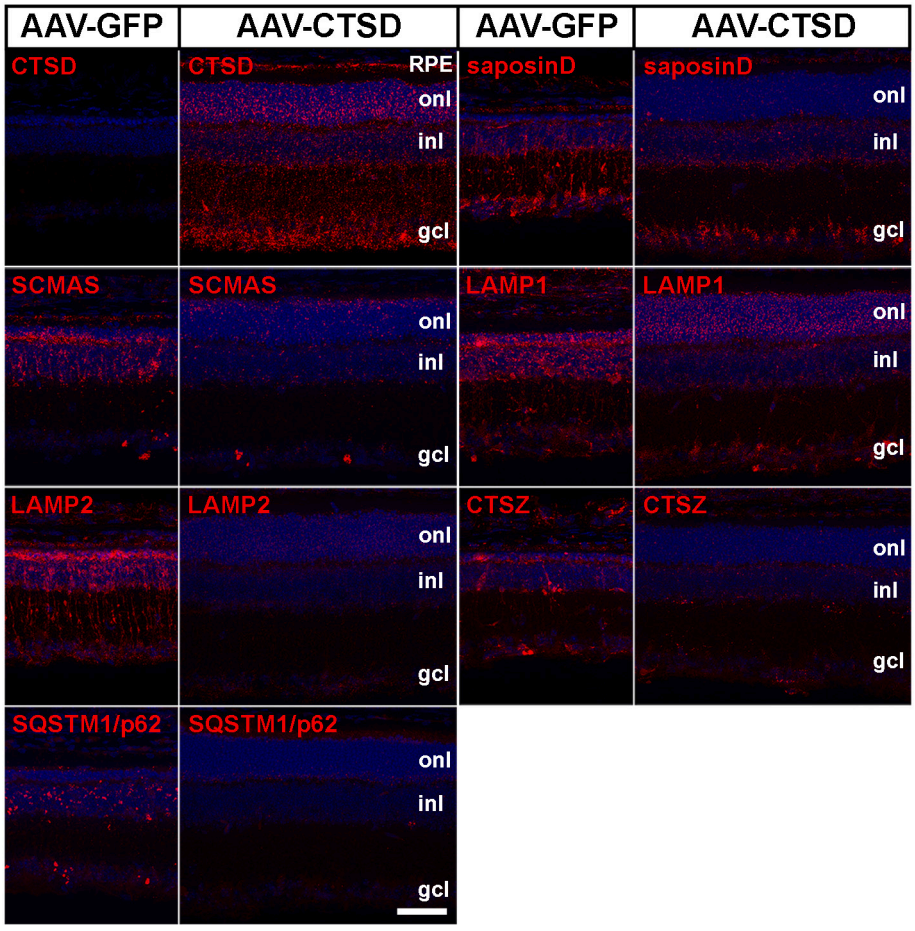

Fig. 4. Impact of intravitreal injections of scAAVshH10-CTSD on the biochemical phenotype of *Ctsd* ko retinas.
Immunohistochemical analyses of retinas from P22 *Ctsd* ko eyes injected with scAAVshH10-CTSD and contralateral control eyes injected with scAAVshH10-GFP with antibodies to CTSD, saposin D, SCMAS, LAMP1, LAMP2, CTSZ and SQSTM1/p62. AAV, adeno-associated virus; CTSD, cathepsin D; CTSZ, cathepsin X/Z/P; gcl, ganglion cell layer; GFP, green fluorescent protein; inl, inner nuclear layer; LAMP1, lysosomal-associated membrane protein 1; LAMP2, lysosomal-associated membrane protein 2; onl, outer nuclear layer; RPE, retinal pigment epithelium; SCMAS, subunit c of mitochondrial ATP synthase; SQSTM1/p62, sequestosome 1/p62. Scale bar, 50 μm. (For interpretation of the references to colour in this figure legend, the reader is referred to the web version of this article.)

control eyes ($p > 0.05$ for all comparisons, paired *t*-test). Similarly, we found no significant difference in the number of PKCα-positive rod bipolar cells or SCGN-positive cone bipolar cells between CTSD-NSC-treated retinas (20.79 ± 0.48/250 μm and 29.36 ± 0.91/250 μm, respectively) and ko-NSC-treated retinas (21.21 ± 0.37/250 μm and 29.5 ± 0.68/250 μm, respectively; $p > 0.05$ for all comparisons, paired *t*-test; Fig. 7A, B). The cell-based treatment thus did not impact the rapidly progressing loss of various retinal cell types.

2.6. CTSD substitution with scAAVshH10-CTSD preserved retina structure in Ctsd ko mice

To investigate whether attenuation of retinal degeneration might be achieved through an AAV vector-mediated gene transfer of CTSD, we explored the impact of the gene therapy treatment on the morphology of *Ctsd* ko retinas. Injections of scAAVshH10-CTSD with a titer of 4,8 × 10^{11} vg/μl had no significant effect on photoreceptor survival in 5 out of 5 treated animals (Fig. S7). Injections of scAAVshH10-CTSD with a titer of 1.2 × 10^{13} vg/μl, in contrast, preserved retina morphology in P22 *Ctsd* ko mice as indicated by the presence of a well-developed outer nuclear layer and numerous cone photoreceptors (Fig. S7). However, in all 4 animals treated with this high AAV titer, eyes were up to 50% smaller than the contralateral control eyes (Fig. S7). In comparison, animals had normally sized eyes and retinal degeneration was markedly attenuated when scAAVshH10-CTSD was injected with a lower titer of 2.5 × 10^{12} vg/μl. 4′,6-diamidino-2-phenylindole (DAPI) staining revealed that the outer nuclear layer of these retinas was significantly thicker when compared to control retinas (Fig. 8A). Quantitative data showed that the number of rows of photoreceptor nuclei was significantly higher in scAAVshH10-CTSD treated eyes (5.60 ± 0.47 rows of nuclei) than in eyes injected with the control vector (1.30 ± 0.15 rows of nuclei; $p < 0.001$, paired *t*-test; Fig. 8B). Rod photoreceptors comprise ~97% of all photoreceptors in the mouse retina (Jeon et al., 1998). Data thus demonstrate that the gene therapy approach effectively promoted rod photoreceptor survival in *Ctsd ko* mice.

Further analyses of the retinal histology showed the presence of numerous m + s opsin-positive or arrestin-positive cone photoreceptors in scAAVshH10-CTSD-treated eyes, while cones were essentially absent from control retinas (Fig. 8A). Surviving cones showed an apparently normal morphology, with well-developed inner and outer segments (Fig. 8A; Fig. S8). Quantitative analysis confirmed a significant protection of cones with 15.74 ± 2.20 (mean ± SEM) m + s opsin-positive cones/250 μm and 12.10 ± 2.55 arrestin-positive cones/250 μm in scAAVshH10-CTSD-treated animals as opposed to 0.38 ± 0.21 m + s opsin-positive cones/250 μm and 0.17 ± 0.08 arrestin-positive cones/250 μm in eyes injected with scAAVshH10-GFP ($p < 0.001$and $p < 0.01$, respectively; paired t-test; Fig. 8B).

Immunostaining of scAAVshH10-CTSD-treated *Ctsd* ko retinas at P22 additionally revealed a more organized morphology of PKCα-positive rod bipolar cells when compared to control retinas (Fig. 8A). In addition, the number of rod bipolar cells in scAAVshH10-CTSD injected retinas was significantly higher (21.98 ± 1.27 (mean ± SEM) cells/250 μm) than in control eyes (17.83 ± 1.21 cells/250 μm; $p < 0.05$, paired t-test; Fig. 8B). The overall morphology of SCGN-positive cone bipolar cells also appeared more organized in scAAVshH10-CTSD-treated retinas than in control retinas (Fig. 8A). However, the number of cone bipolar cells in scAAVshH10-CTSD-treated retinas at P22 (30.75 ± 1.99 (mean ± SEM) cone bipolar cells/250 μm) was not significantly different from that found in control eyes (27.92 ± 1.45 cone bipolar cells/250 μm; $p > 0.05$, paired t-test; Fig. 8B).

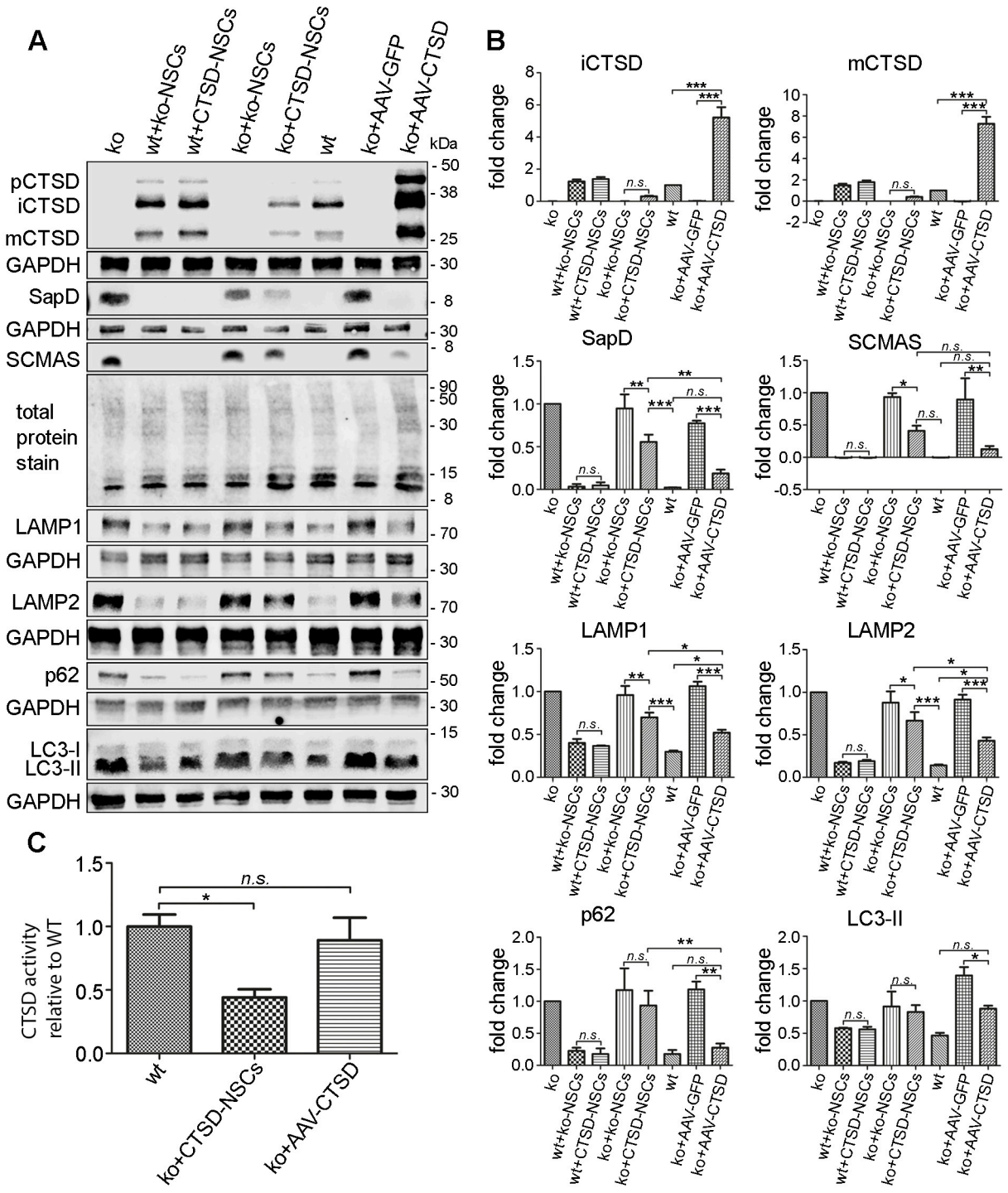

Fig. 5. Immunoblot analysis and CTSD activity assay of *Ctsd* ko retinas treated with NSCs or AAV vectors.
Western blot analyses of CTSD, saposin D, SCMAS, LAMP1, LAMP2, SQSTM1/p62 and LC3 in untreated or treated *Ctsd* ko or *Ctsd* wt retinas at P22. (B) Quantitative analyses of immunoblots. Bars represent the mean (±SEM) of 3 independent experiments. CTSD levels were normalized to those in untreated wt retinas, while levels of all other antigens were normalized to those in untreated ko retinas. *, $p < 0.05$, **, $p < 0.01$, and ***, $p < 0.001$; n.s., not significant; one-way ANOVA. (C) CTSD enzymatic activity in P22 untreated *Ctsd* wt retinas, and *Ctsd* ko retinas treated with NSCs or AAV vectors. Each bar represents the mean ± SEM of 6 retinas. *, $p < 0.05$; n.s., not significant; one-way ANOVA. AAV, adeno-associated virus; CTSD, cathepsin D; GAPDH, glyceraldehyde-3-phosphate dehydrogenase; GFP, green fluorescent protein; iCTSD, intermediate-CTSD; ko, knockout; ko + ko-NSCs, *Ctsd* ko retinas treated with ko-NSCs; ko + CTSD-NSCs, *Ctsd* ko retinas treated with CTSD-NSCs; ko + AAV-GFP, *Ctsd* ko retinas treated with scAAVshH10-GFP; ko + AAV-CTSD, *Ctsd* ko retinas treated with scAAVshH10-CTSD; LAMP1, lysosomal-associated membrane protein 1; LAMP2, lysosomal-associated membrane protein 2; LC3-I/II, microtubule-associated protein 1 light chain 3-I/II; mCTSD, mature-CTSD; NS, neural stem cells; pCTSD, pro-CTSD; SapD, saposin D; SCMAS, subunit c of mitochondrial ATP synthase; wt, wild-type; wt + ko-NSCs, *Ctsd* wt retinas treated with ko-NSCs; wt + CTSD-NSCs, *Ctsd* wt retinas treated with CTSD-NSCs. (For interpretation of the references to colour in this figure legend, the reader is referred to the web version of this article.)

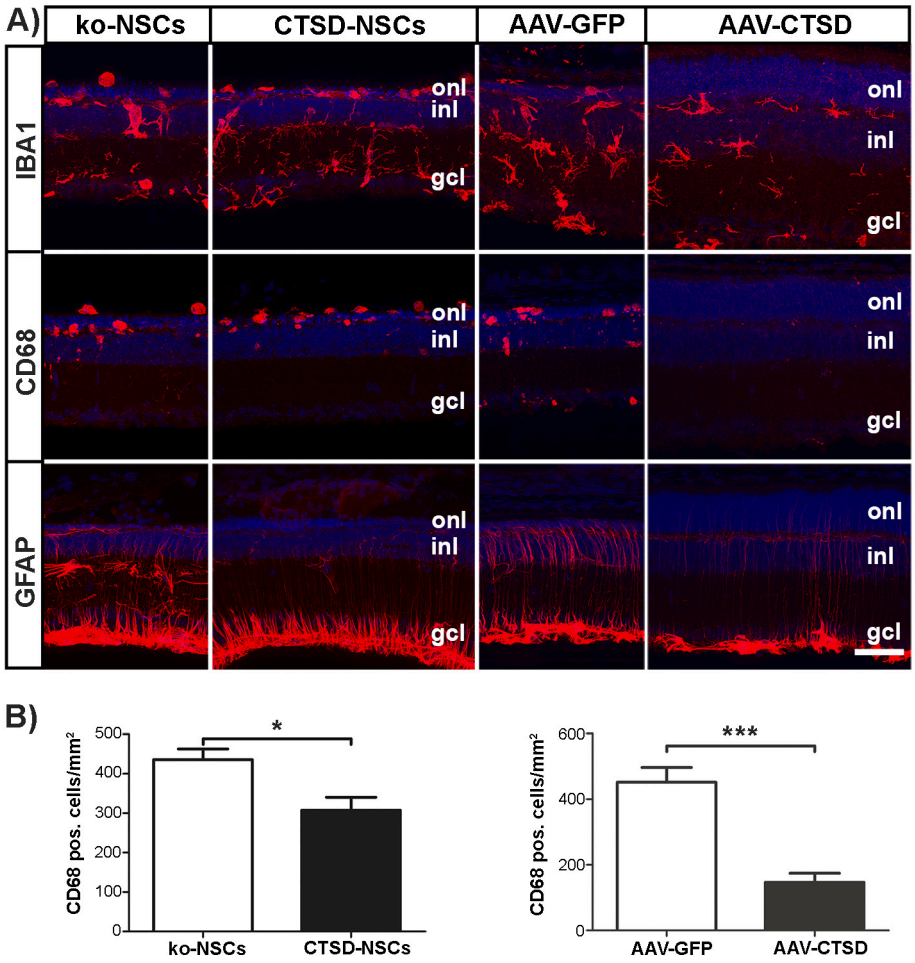

Fig. 6. Attenuation of reactive microgliosis and astrogliosis in *Ctsd* ko retinas treated with NSCs or AAV vectors.
(A) Immunostainings of IBA1-positive microglia cells, CD68-positive microglia/macrophages, and GFAP-positive Müller cells and astrocytes in NSC-treated (CTSD-NSCs), AAV-treated (AAV-CTSD) and respective control *Ctsd* ko retinas (ko-NSCs and AAV-GFP). (B) The density of CD68-positive cells in P22 *Ctsd* ko retinas treated with either NSCs or AAV vectors. Each bar represents the mean value (±SEM) of 6 animals. *, $p < 0.05$, ***, $p < 0.001$; paired t-test. AAV, adeno-associated virus; CD68, cluster of differentiation 68; CTSD, cathepsin D; gcl, ganglion cell layer; GFAP, glial fibrillary acidic protein; GFP, green fluorescent protein; IBA1, ionized calcium-binding adapter molecule 1; inl, inner nuclear layer; ko, knockout; NSCs, neural stem cells; onl, outer nuclear layer. Scale bar, 50 μm. (For interpretation of the references to colour in this figure legend, the reader is referred to the web version of this article.)

3. Discussion

Brain-directed enzyme substitution therapies have been demonstrated to attenuate brain atrophy and deterioration of neurological symptoms in NCLs caused by dysfunctional lysosomal enzymes, both in animal models (Geraets et al., 2016; Johnson et al., 2019; Kohlschutter et al., 2019; Neverman et al., 2015) and patients (Schaefers et al., 2021; Schulz et al., 2018; Sondhi et al., 2020). Importantly however, the brain-directed treatments had no beneficial impact on the retinal pathology. An AAV-mediated *Ctsd* gene transfer to the brain of neonatal CTSD-deficient mice, for instance, effectively delayed disease progression in the brain and viscera and markedly prolonged the life span of the mutant mice but had no impact on the progression of the retinal dystrophy (Shevtsova et al., 2010). Similarly, an AAV-mediated administration of TPP1 to the brains of CLN2 patients attenuated brain atrophy and deterioration of neurological symptoms, but not retinal degeneration (Sondhi et al., 2020). These findings indicate the need to combine eye-directed and brain-directed enzyme substitution therapies in order to attenuate both, retinal degeneration and brain atrophy. Until now, however, only few studies have evaluated the use of enzyme substitution strategies as treatment options for retinal dystrophies in these conditions (Griffey et al., 2005; Tracy et al., 2016; Whiting et al., 2020a; Whiting et al., 2020b). We have recently analyzed the impact of an enzyme replacement therapy on the retinal pathology in *Ctsd* ko mice. While the treatment partially corrected lysosomal and autophagic dysfunction, it had no impact on the rapidly progressing loss of retinal nerve cells (Marques et al., 2020), presumably due to insufficient amounts of enzymatically active CTSD. In the present work, we therefore evaluated the outcome of a sustained intraocular administration of CTSD using intravitreal injections of a CTSD overexpressing NSC line or a CTSD encoding AAV vector.

For the cell-based administration of CTSD, we generated a clonal NSC line with a stable overexpression of the zymogen. The modified NSCs and astrocytes derived from these stem cells released more pCTSD into the culture supernatant and contained higher levels of enzymatically active CTSD than the corresponding wt cell types. In CTSD uptake experiments, the protease released from the modified cells was found in CTSD-deficient astrocytes where it was co-localized with LAMP1 and LAMP2 and processed to iCTSD, indicating correct trafficking to the endolysosomal compartment and proteolytic activation. Decreased levels of LAMP1 and LAMP2 in the treated cells additionally indicated amelioration of the lysosomal hypertrophy. CTSD uptake by various nerve cell types and glial cells was also observed in *Ctsd* ko primary retinal cell cultures maintained in conditioned medium from CTSD-astrocytes.

CTSD-NSCs were intravitreally grafted into *Ctsd* ko mice at P7 prior to the onset of retinal degeneration (Bassal et al., 2021). In the treated eyes, CTSD was found throughout the entire thickness of the retinas, and CTSD enzymatic activity was restored to ~44% of normal at the end stage of the disease at P22. Results demonstrate release of pCTSD from the grafted cells into the aqueous humour, diffusion into the retina, and correct trafficking and processing in retinal cells. Partial clearance of storage material as revealed by significantly decreased levels of saposin D and SCMAS confirmed successful delivery of CTSD to the dystrophic retina. Reduced levels of LAMP1, LAMP2 and CTSZ in the neuroretina additionally indicated amelioration of the lysosomal hypertrophy, an

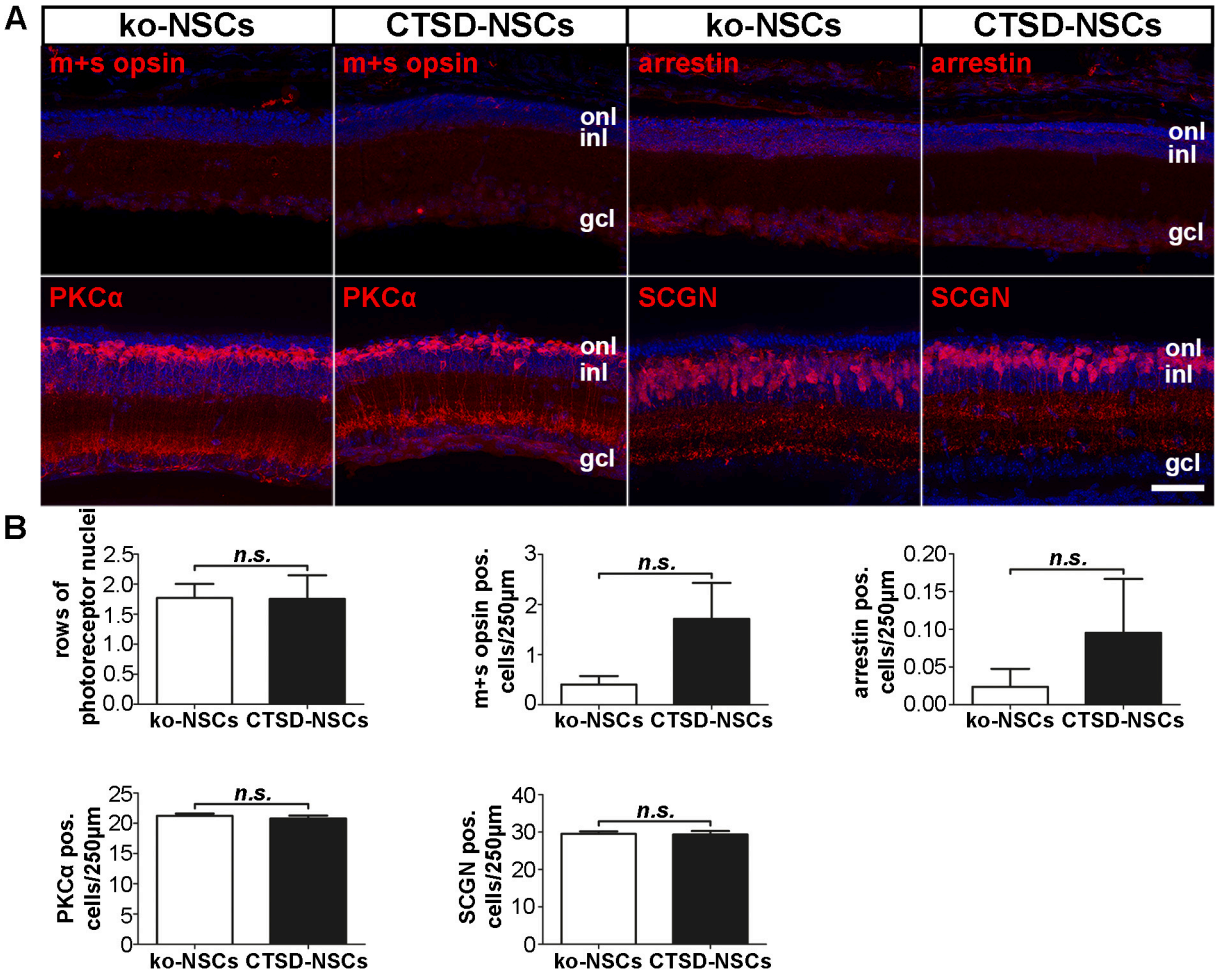

Fig. 7. The impact of intravitreally grafted CTSD-NSCs on photoreceptor and bipolar cell survival in *Ctsd ko* retinas.
(A) Immunostainings of P22 *Ctsd* ko retinas treated with CTSD-NSCs and contralateral retinas treated with ko-NSCs using antibodies to m + s opsin, arrestin, PKCα and SCGN. (B) The number of rows of photoreceptor nuclei and m + s opsin-, arrestin-, PKCα-, and SCGN-positive cells per 250 µm retina length in P22 *Ctsd* ko retinas treated with ko-NSCs or CTSD-NSCs. Each bar represents the mean value (±SEM) of 7 animals. n.s., not significant; paired t-test. CTSD, cathepsin D; gcl, ganglion cell layer; inl, inner nuclear layer; ko, knockout; NSCs, neural stem cells; onl, outer nuclear layer; PKC*α*, protein kinase C-alpha; SCGN, secretagogin. Scale bar, 50 µm.

adaptive response to lysosomal stress in part controlled by the transcription factor EB (TFEB) (Ballabio and Bonifacino, 2020; Sardiello et al., 2009; Settembre and Ballabio, 2014). Levels of LAMP1 and LAMP2 in the RPE were, however, not markedly different in eyes with grafted CTSD-NSCs or ko-NSCs. Immunostainings of untreated *Ctsd* ko retinas revealed the presence of p62 bodies in diverse nerve cell types, including cone photoreceptors and rod and cone bipolar cells. Immunoblot analyses confirmed elevated levels of SQSTM1/p62, indicating dysfunction of lysosomes followed by accumulation of autophagic cargo and thus disruption of the autophagic flux. Furthermore, increased levels of lipidated LC3 in untreated mutant retinas indicated accumulation of autophagosomes presumably as a result of impaired autophagosome-lysosome fusion in the multistep autophagic pathway, as demonstrated in the brain and retina of *Ctsd* ko mice and in animal models of other NCLs (Atiskova et al., 2019; Bassal et al., 2021; Koike et al., 2005; Thelen et al., 2012; von Eisenhart-Rothe et al., 2018). While immunohistochemistry suggested a decrease in the number of p62 bodies, immunoblot analyses revealed similar levels of SQSTM1/p62 and lipidated LC3 in CTSD-NSC treated and control retinas. Despite restoration of CTSD enzymatic activity to more than 40% of wild-type level, the treatment thus only partially corrected the lysosomal dysfunction and had no beneficial impact on the disrupted autophagic flux. These apparently discrepant findings might be related to (i) a preferential uptake of pCTSD from the aqueous humour by only a subpopulation of retinal cells such as Müller cells and astrocytes which form the inner limiting membrane facing the vitreous cavity and/or cell types located in the inner retina and thus close to the vitreous cavity, such as ganglion cells and displaced amacrine cells and/or (ii) only slowly increasing CTSD amounts in the mutant retinas, resulting in activity levels insufficient to more effectively correct the biochemical phenotype during early phases of the retinal dystrophy.

To treat the early-onset retinal dystrophy in *Ctsd* ko mice with a gene therapy approach, we used a self-complementary AAV vector to assure rapid transgene expression. Furthermore, we used an AAVshH10 serotype which shows a selective tropism to Müller cells (Klimczak et al., 2009), radial glia cells which span the entire thickness of the retina, anticipating that infection of these cells will result in widespread distribution of CTSD in the mutant retina. AAVshH10 also shows a tropism to RPE cells (Gonzalez-Cordero et al., 2018), phagocytically active cells which play a pivotal role for photoreceptor function and survival. AAVs were intravitreally injected into *Ctsd* ko mice at P5. At this age, diffusion of viral particles into the developing retina is not impeded by a fully mature inner limiting membrane (Dalkara et al., 2009; Kleine Holthaus et al., 2018). Expression of CTSD or GFP was indeed clearly evident in Müller cells and RPE cells as early as 4 days after intravitreal injections of AAV particles, and thus prior to the onset of significant retinal

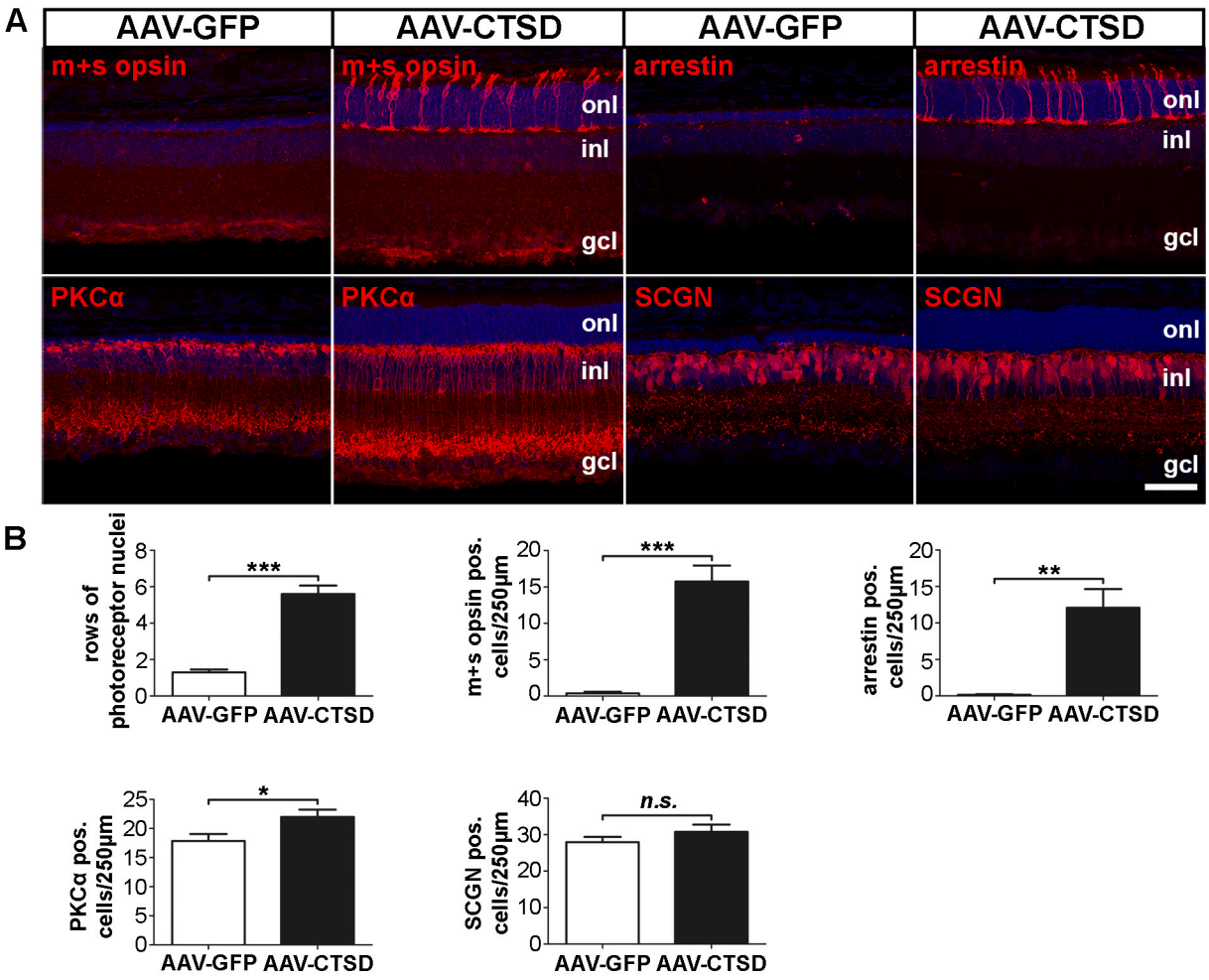

Fig. 8. The impact of intravitreally injected scAAVshH10-CTSD on photoreceptor and bipolar cell survival in *Ctsd ko* retinas.
(A) Immunostainings of P22 *Ctsd* ko retinas treated with scAAVshH10-CTSD and contralateral retinas treated with scAAVshH10-GFP using antibodies to m + s opsin, arrestin, PKCα and SCGN. (B) The number of rows of photoreceptor nuclei and m + s opsin-, arrestin-, PKCα-, and SCGN-positive cells per 250 µm retina length in P22 retinas treated with scAAVshH10-GFP or scAAVshH10-CTSD. Each bar represents the mean value (±S.E.M.) from 7 animals. Statistical analyses were performed with the paired t-test. *, $p < 0.05$, **, $p < 0.01$, ***, $p < 0.001$; n.s., not significant. AAV, adeno-associated virus; CTSD, cathepsin D; gcl, ganglion cell layer; GFP, green fluorescent protein; inl, inner nuclear layer; onl, outer nuclear layer; PKC*α*, protein kinase C-alpha; SCGN, secretagogin. Scale bar, 50 µm. (For interpretation of the references to colour in this figure legend, the reader is referred to the web version of this article.)

degeneration between P10 and P15 (Bassal et al., 2021). However, at this early age CTSD was expressed at relatively low levels and in an inhomogeneous pattern. In older animals, in comparison, the protease was detectable in all retinal cell types, demonstrating release of the enzyme from retinal glial cells and RPE cells and subsequent uptake by neighboring non-modified cell types, a process referred to as cross correction. Notably, levels of iCTSD and mCTSD in treated retinas were markedly increased by a factor of 5.2 and 7.3, respectively when compared to wild-type retinas, and CTSD enzymatic activity was restored to levels similar to those found in normal healthy retinas. Prevention of storage material accumulation and significantly reduced expression levels of LAMP1 and LAMP2 indicated almost complete correction of the lysosomal dysfunction in the mutant neuroretina. Levels of LAMP2, but not LAMP1, were also markedly decreased in the RPE. Importantly, and in difference to NSC-treated retinas, AAV-treated retinas were devoid of p62 bodies. Immunoblot analyses confirmed complete clearance of SQSTM1/p62 and revealed a decrease of lipidated LC3 to levels not significantly different from those in wild-type retinas. The combined results thus indicate nearly complete restoration of the impaired autophagy-lysosomal pathway in AAV-treated *Ctsd* ko retinas.

Based on the finding that reactive microgliosis and astrogliosis closely accompanies or even precedes neurodegeneration in different NCLs, neuroinflammation has been implicated in the progression of the neurological pathology in these conditions. In support of this view, anti-inflammatory therapies have been shown to ameliorate the neurological phenotype of various NCL animal models (Bosch and Kielian, 2015; Kohlschutter et al., 2019; Palmer et al., 2013), and to partly preserve retina structure (Groh et al., 2017; Mirza et al., 2013). Notably, reactive microglia cells have also been demonstrated to promote neurodegeneration in the brain and inner retina of *Ctsd* ko mice through overproduction of nitric oxide in response to a storage-induced activation of p38 mitogen-activated protein kinase (Koike et al., 2003; Nakanishi et al., 2001; Yamasaki et al., 2007). The present study revealed that both, the NSC- and the AAV-mediated administration of CTSD resulted in reduced densities of IBA1- and CD68-positive cells and reduced levels of GFAP in retinal glial cells. However, attenuation of neuroinflammation was markedly more pronounced in AAV-treated retinas than in NSC-treated retinas, as indicated by a ramified rather than an amoeboid morphology of the majority of IBA1-positive microglia cells, and a more pronounced decrease in the density of CD68-positive microglia/macrophages.

While the cell-based treatment partially prevented storage

accumulation and lysosomal hypertrophy, it had no impact on the rapidly progressing loss of retinal nerve cells, similar to our results obtained with an enzyme replacement therapy (Marques et al., 2020). The combined results suggest that relatively large amounts of CTSD are required to promote neuronal survival in the mutant retina. In apparent difference, restoration of enzymatic activity of the lysosomal enzymes palmitoyl-protein thioesterase 1 (PPT1) or TPP1 to 10% or less of normal appears to be sufficient to ameliorate progression of CLN1 and CLN2 disease respectively, as indicated by enzyme substitution experiments on *Ppt1* ko mice, genotype-phenotype correlations in CLN2 patients, or analyses of hypomorphic CLN2 mice (Sleat et al., 2008; Sleat et al., 1999; Sondhi et al., 2020; Tamaki et al., 2009). In any case, restoration of CTSD enzymatic activity close to wild-type levels achieved with the gene therapy approach correlated with a marked rescue of various retinal cell types. Preservation of retina structure was most obviously revealed by the presence of numerous rod and cone photoreceptor cells in treated retinas as opposed to the almost complete loss of these cells in control retinas. The gene therapy treatment also rescued rod bipolar cells from cell death, while numbers of cone bipolar cells were similar in treated and control retinas at P22. The late loss of cone bipolar cells between P20 and P25 (Bassal et al., 2021) provides an explanation for the latter observation. Importantly, we also found that injections of scAAVshH10-CTSD with a titer of 1.2×10^{13} vg/µl resulted in marked atrophy of the treated eyes. Similar adverse effects were not observed in any of the animals treated with lower AAV titers or NSCs. While the cause of this severe complication is unknown, it highlights the need to precisely control the dosing of CTSD in therapeutic interventions. Of interest in this context, excessive levels of cytosolic or extracellular CTSD have been implicated in ocular diseases and various other disorders including cancer (Benes et al., 2008; Lakkaraju et al., 2020; Mijanovic et al., 2021; Yadati et al., 2020).

Photoreceptor outer segments (POS) are constantly renewed. One critical function of RPE cells is the phagocytosis and degradation of the daily shedded POS tips (Lakkaraju et al., 2020; Strauss, 2005). Failure of POS phagocytosis or impaired POS degradation causes photoreceptor degeneration (D'Cruz et al., 2000; Jiang et al., 2015; Karan et al., 2005). Once POS tips are ingested, phagosomes mature along the endocytic pathway to finally fuse with lysosomes (Wavre-Shapton et al., 2014). As reviewed in detail elsewhere (Intartaglia et al., 2021; Lakkaraju et al., 2020), a significant fraction of POS phagosomes is degraded *via* a non-canonical autophagy pathway referred to as LC3-associated phagocytosis (LAP). In LAP, LC3 associates with POS phagosomes in an Atg5- and Beclin1-dependent manner, thus linking part of the autophagy machinery to POS phagocytosis (Kim et al., 2013). CTSD plays a major role in the degradation of POS proteins as exemplified, for instance, by the accumulation of POS-derived debris in RPE cells of a transgenic mouse expressing an enzymatically inactive CTSD variant (Rakoczy et al., 2002; Zhang et al., 2002). Rapid onset and robust expression of CTSD in RPE cells achieved with the AAVshH10 serotype thus likely contributes to the marked promotion of photoreceptor survival in the *Ctsd* ko retina by ameliorating impaired POS degradation through classical phagocytosis and LAP in addition to autophagy dysfunction.

Surviving photoreceptors in AAV-treated retinas displayed an apparently normal morphology, and rod and cone bipolar cells also showed a better morphological organization than in control eyes. However, it remains unknown whether the gene therapy treatment preserved retina function in addition to retina structure, since we were unable to perform electroretinogram (ERG) recordings due to ethical concerns related to the severe phenotype of the mice at advanced stages of the disease at P22. Of interest in this context, an AAV2-mediated expression of the lysosomal enzyme PPT1 in the retina of *Ppt1* ko mice has been shown to attenuate deterioration of visual function as assessed in ERG recordings (Griffey et al., 2005). Preservation of retina function and structure was also observed in a CLN2 canine model after a single intravitreal injection of TPP1-overexpressing mesenchymal stem cells (Tracy et al., 2016) or repeated intravitreal injections of recombinant TPP1 (Whiting et al., 2020a; Whiting et al., 2020b). These studies together with the present work suggest that eye-directed enzyme substitution therapies show promise for the treatment of retinal dystrophies in a subgroup of NCLs.

4. Materials and methods

4.1. Animals

C*tsd* ko mice (Saftig et al., 1995) were derived from heterozygous breeding pairs maintained on a C57BL/6 J genetic background. Genotypes of animals were determined by polymerase chain reaction (PCR) using forward primer 5'-GTC ACC TGC AGC TTT GGT A-3′ and reverse primer 5'-TCA GCT GTA GTT GCT CAC ATG-3′. Wt littermates were used as a control. All animals were housed under standard conditions with *ad libitum* access to food and water. All animal experiments were approved by the local ethic committee (077/2019) and were carried out in accordance with the EU directive guidelines for animal experiments.

4.2. Generation of lentivirally modified clonal neural stem cell lines

To generate a CTSD overexpressing clonal NSC line, murine full-length CTSD cDNA was cloned into a polycistronic lentiviral vector composed of a cytomegalovirus enhancer/chicken ß-actin (CAG) hybrid promoter, the internal ribosome entry site (IRES) of the encephalomyocarditis virus, a tdTomato reporter gene and a blasticidin (BSD) resistance gene, giving rise to pCAG-CTSD-IRES-tdTomato-BSD. The vector was used to establish a CTSD-NSC clone. The same vector but lacking the CTSD cDNA (pCAG-IRES-tdTomato-BSD) was used to generate a clonal NSC line as a control for *in vitro* experiments (wt-NSCs). As another control cell line for *in vitro* and *in vivo* experiments, a clonal *Ctsd* ko NSC line was established using a vector composed of the elongation factor-1 α promoter, an IRES sequence, and a Venus reporter gene separated from a puromycin resistance gene by a P2A sequence of porcine teschovirus-1 (ko-NSCs). In addition, we used nonmodified Venus-negative *Ctsd* ko astrocytes in CTSD uptake experiments. Lentiviral particles were prepared by transient transfection of human embryonic kidney (HEK) 293 T cells as described (http://www.LentiGo-Vectors.de). Clonally derived NSC lines were established and cultivated as described (Flachsbarth et al., 2014; Jung et al., 2013). In brief, successfully transduced cells were expanded in the presence of either 4 µg/ml BSD or 0.6 µg/ml puromycin (both from Life Technologies, Darmstadt, Germany), and single cells with high levels of reporter gene expression were sorted into 96 well plates by fluorescence activated cell sorting (FACS; FACS Arialllu, BD Bioscience, San Diego, CA, USA), followed by clonal expansion.

4.3. Production and titration of AAV particles

AAVshH10 pseudotyped vectors (Klimczak et al., 2009) were generated by co-transfection of HEK293T-AAV cells (293AAV; Cell Biolabs, San Diego, USA) with the AAV transfer plasmid scAAV-CMV-CTSD and the AAV packaging plasmid shH10 (shH10 was a gift from John Flannery & David Schaffer to the Bartsch lab, Addgene plasmid # 64867) and pHelper (Cell Biolabs). 293AAV cells were cultivated in Dulbecco's modified Eagle's medium (DMEM; Life Technologies) supplemented with 10% (*v*/v) heat-inactivated fetal calf serum, 0.1 mM MEM, Non-Essential Amino Acids (Life Technologies), 100 U/ml penicillin and 100 µg/ml streptomycin. Briefly, 10^7 293AAV cells were seeded one day before transfection on 15 cm culture dishes and transfected with 7.5 µg packaging plasmid shH10, 10 µg pHelper and 6.4 µg pAAV plasmid scAAV-CMV-CTSD or 7.1 µg scAAV-CMV-CTSD-E2A-GFP per plate complexed with Polyethylenimine "Max" (PEI MAX, MW 40,000; Polysciences, Warrington, PA, USA) at a PEI:DNA ratio (*w*/w) of 3:1 (Fukumoto et al., 2010). After 72 h, cells were harvested and resuspended in 5 ml lysis buffer (50 mM Tris base, 150 mM NaCl, 5 mM

$MgCl_2$, pH 8.5). After three freeze-thaw cycles, Turbo Nuclease (Th. Geyer, Renningen, Germany) was added and the lysates were incubated for 1 h at 37 °C. Cell debris was pelleted and vector containing lysates were purified using iodixanol step gradients (PROGEN Biotechnik GmbH, Heidelberg, Germany). Finally, iodixanol was removed by ultrafiltration using Amicon Ultra Cartriges (MerckMillipore, Darmstadt, Germany).

The genomic titers of DNAse-resistant recombinant AAV particles were determined after alkaline treatment of virus particles and subsequent neutralization by qPCR using the qPCRBIO SY Green Mix Hi-Rox (Nippon Genetics Europe GmbH, Düren, Germany) and an ABI PRISM 7900HT cycler (Applied Biosystems, Waltham, MA, USA). Vectors were quantified using primers specific for the CMV promoter sequence (5'-GGGACTTTCCTACTTGGCA and 5′-ctaccgcccatttgcgtc). Real-time PCR was performed in a total volume of 10 µl with 0.3 µM of each primer. The corresponding scAAV transfer plasmid was used as a copy number standard. A standard curve for quantification was generated by serial dilutions of the respective plasmid DNA. The cycling conditions were as follows: 50 °C for 2 min, 95 °C for 10 min, followed by 35 cycles of 95 °C for 15 s and 60 °C for 60 s. Calculations were done using the SDS 2.4 software (Applied Biosystems).

4.4. In vitro differentiation of NSCs and primary retinal cell culture

Differentiation of CTSD-NSCs, wt-NSCs and ko-NSCs into astrocytes and neurons was performed as described previously (Jankowiak et al., 2015). For primary retinal cell cultures, retinas from 2 days old *Ctsd* ko mice were dissociated with Accutase (Life Technologies) for 5–10 min at 37 °C, and centrifuged at 1400 rpm for 7 min. Cell pellets were resuspended in astrocyte differentiation (AD) medium consisting of DMEM/F12 (Life Technologies) supplemented with 2 mM L-glutamine, 0.3% glucose, 5 mM 4-(2-hydroxyethyl)-1-piperazineethanesulfonic acid (HEPES; Roth, Karlsruhe, Germany), 3 mM sodium bicarbonate, 1% fetal calf serum and 2% B27 (all from Life Technologies), filtered through a 40 µm Falcon Cell Strainer (VWR International, Erlangen, Germany) and cultivated at a density of 220,000 cells/cm^2 on Matrigel-coated coverslips in AD medium for 9 days.

4.5. CTSD uptake experiments

To analyze CTSD uptake in co-culture experiments, tdTomato-positive CTSD-NSCs and Venus-negative ko-NSCs were mixed 1:1 and cultured in DMEM/F12 containing 2 mM L-glutamine, 0.3% glucose, 5 mM HEPES, 3 mM sodium bicarbonate, 10 ng/ml epidermal growth factor and 10 ng/ml fibroblast growth factor-2 (both from TEBU, Offenbach, Germany) and 1% B27 and 1% N2 (Life Technologies). After 3 days, cells were differentiated into astrocytes in AD medium, cultured for additional 7 days, harvested using Accutase, and reseeded onto coverslips for CTSD immunocytochemistry. Pure ko-astrocyte cultures served as a negative control.

To analyze CTSD uptake from conditioned media, culture supernatants from CTSD-astrocytes or ko-astrocytes were collected every second day, filtered using 0.45 µm filters (Sarstedt, Nümbrecht, Germany) and stored at −80 °C until use. ko-astrocytes or primary retinal cells from *Ctsd* ko mice were cultured in conditioned media collected from either CTSD-astrocytes or ko-astrocytes for 7 days. Conditioned media were changed every second day.

4.6. Intravitreal NSC transplantations and intravitreal AAV injections

NSCs and AAV particles were intravitreally injected into 7 and 5 days old mice, respectively as described (Flachsbarth et al., 2014; Jankowiak et al., 2015; Jung et al., 2013). 3.8×10^5 CTSD-NSCs in 1 µl PBS or 1 µl of scAAVshH10-CTSD (2.5×10^{12} vg/µl) was injected into the right eyes. The contralateral eye of each animal served as a control and received injections of 3.8×10^5 ko-NSCs in 1 µl PBS or 1 µl of scAAVshH10-GFP (2.5×10^{12} vg/µl). Due to ethical concerns, animals were sacrificed at P22 before the appearance of a severe neurological phenotype. For morphological and immunoblot analyses, we intravitreally grafted CTSD-NSCs and ko-NSCs into 19 *Ctsd* ko mice and 11 wild-type mice, and injected scAAVshH10-CTSD and scAAVshH10-GFP into the vitreous cavity of 20 *Ctsd* ko mice. From these animals, 3 mutant and 2 wild-type mice with grafted NSCs and 4 mice with injected AAVs had to be excluded due to complications associated with the injections such as retinal damage, retinal bleeding or reflux of cells or viral particles. We additionally used 9 *Ctsd* ko mice to determine an optimal AAV titer.

4.7. Western blot analyses and enzyme activity assay

Cultured cells or retinas were homogenized in lysis buffer containing 50 mM Tris-HCl, pH 7.5, 150 mM NaCl, 0.5% Triton-X100 and protease inhibitors, and incubated on ice for 15 min. After centrifugation for 10 min at x20,000 g, supernatants were collected. For detecting SQSTM1/p62, saposin D and MAP1LC3-I/II, retinas were sonified in radioimmunoprecipitation assay buffer containing 50 mM Tris-HCl, pH 7.4, 150 mM NaCl, 1% Triton-X100, 0.5% sodium deoxylcholate, 0.1% sodium dodecyl sulfate (SDS; Merck Millipore), 1 mM ethylenediaminetetraacetic acid (EDTA; Roth), 10 mM sodium fluoride, 1 mM phenylmethylsulfonyl fluoride and protease inhibitors, centrifuged at 13,000 *g* for 15 min at 4 °C and supernatants were collected. Preparation of detergent-insoluble fractions for detecting SCMAS was performed as described (Jankowiak et al., 2016). Protein concentrations were determined using the bicinchoninic acid assay (Roth). Samples were separated by 10%, 15% or 10%–20% SDS-PAGE gel electrophoresis, transferred onto nitrocellulose membranes or polyvinylidene fluoride membranes, and processed for immunoblotting as described (Atiskova et al., 2019). Glyceraldehyde 3-phosphate dehydrogenase or Revert™ 700 Total protein stain (LI-COR Biosciences, Lincoln, NE, USA) was used as a loading control. Blots were analyzed using the Odyssey® Fc Imaging System, and signals within the linear range of detection were quantified using Empiria Studio® Software 1.2.0.79 (LI-COR Biosciences). Chameleon Duo Pre-stained Protein Ladder (LI-COR Biosciences, 928–60,000) was used to determine molecular masses. Each experiment was performed at least in triplicate.

For determination of CTSD enzymatic activity, pellets from NSC cultures and untreated and experimentally treated retinas were lysed for 1 h in PBS containing 0.2% Triton X-100 on a shaker. Lysates were clarified by centrifugation and protein concentrations were determined with the BCA Protein Assay. 2.5 µg of cell lysates or 5 µg of retina lysates were incubated at 37 °C in activity buffer (50 mM sodium acetate, pH 5.5, 0.1 M NaCl, 1 mM EDTA, and 0.2% Triton X-100) containing 10 µM of CTSD and E substrate (Enzo Life Sciences, Lörrach, Germany) and 25 µM leupeptin. The AMC released as a result of proteolytic activity was quantified with a Synergy™ HT Multi-Detection microplate reader (excitation: 360 nm; emission: 440 nm, band pass 40). 2 µl of purified enzymatically active CTSD was used as a positive control, and 2 µl of enzymatically active CTSD in the presence of 1.4 µM Pepstatin A was used as a negative control.

4.8. Immunocytochemistry and immunohistochemistry

For immunocytochemical analyses, cell cultures were fixed in PBS (pH 7.4) containing 4% paraformaldehyde for 10–15 min, blocked for 1 h in PBS containing 0.1% bovine serum albumin (Sigma-Aldrich, St. Louis, MO, USA) and 0.3% Triton X-100, and incubated with primary antibodies (Table S1) overnight, followed by incubation with Cy2-, Cy3- or Cy5-conjugated secondary antibodies (1:200; all from Jackson Immunoresearch Laboratories, West Grove, PA, USA) for 4 h. Cell nuclei were stained with DAPI (Sigma-Aldrich, B2883). Immunostainings of retinal sections were performed as described (Atiskova et al., 2019; Bartsch et al., 2013; Jankowiak et al., 2016). At least six animals were analyzed for each antigen and experimental group. To allow for direct

comparison of staining intensities, sections from treated and contralateral control eyes were processed in parallel in each experiment.

Images from immunostained cell cultures and retinal sections were taken with an AxioObserverZ.1 microscope equipped with an ApoTome.2 and ZEN2.3 software (Zeiss, Oberkochen, Germany) using a x40 oil objective. Since analyses of dorsal, ventral, temporal and nasal retina regions revealed no heterogeneity in the progression of retinal degeneration, we performed all morphological studies on central (*i.e.* in the plane of the optic disc) retinal sections with a nasal-temporal orientation. Rows of photoreceptor cell nuclei were counted in 9 equidistant positions in both the nasal and temporal retinal half in sections stained with DAPI. Arrestin-, m + s opsin-, PKCα- and SCGN-positive cells were counted in 3 equidistant areas each with a width of 250 μm in both the nasal and the temporal retinal half. The number of CD68-positive cells was determined in entire central retina sections. PKCα-, SCGN- and CD68-positive cells were counted in optical sections with a thickness of 0.24 μm, while m + s opsin- or arrestin-positive cone photoreceptor cells were counted in z-stacks through the entire retina thickness.

4.9. Statistical analyses

The density of retinal cell types in treated and contralateral control retinas was compared with the paired Student's *t*-test. Statistical analyses of data from immunoblots and CTSD activity assays were performed with the unpaired Student's t-test or the one-way ANOVA followed by the Newman-Keuls test using Prism 5.02 software (GraphPad Software, San Diego, CA, USA).

CRediT authorship contribution statement

Junling Liu: Conceptualization, Methodology, Investigation, Data curation, Writing – original draft, Funding acquisition, writing - review & editing. **Mahmoud Bassal**: Methodology, Investigation, writing - review & editing. **Stefanie Schlichting**: Methodology, Investigation. **Ingke Braren**: Methodology, writing - review & editing. **Alessandro Di Spiezio**: Methodology, Investigation, Data curation. **Paul Saftig**: Resources, Data curation, Funding acquisition, writing - review & editing. **Udo Bartsch**: Conceptualization, Resources, Data curation, Writing – original draft, Supervision, writing - review & editing.

Declaration of Competing Interest

The authors declare no competing interests

Acknowledgments

The authors are grateful to Elke Becker and Sabine Helbing for excellent technical assistance, Ali Derin and Susanne Conrad for animal care, and Susanne Bartsch and Stephan Storch for helpful discussions and critically reading the manuscript. L.J. is supported by the China Scholarship Council (201708310088), P.S. by the Deutsche Forschungsgemeinschaft (SFB877) and A.D.S. by intramural funding of the Medical Faculty, CAU Kiel.

Appendix A. Supplementary data

Supplementary data to this article can be found online at https://doi.org/10.1016/j.nbd.2022.105628.

References

Adams, J., et al., 2019. Autophagy-lysosome pathway alterations and alpha-synuclein up-regulation in the subtype of neuronal ceroid lipofuscinosis, CLN5 disease. Sci. Rep. 9, 151.
Atiskova, Y., et al., 2019. Mice deficient in the lysosomal enzyme palmitoyl-protein thioesterase 1 (PPT1) display a complex retinal phenotype. Sci. Rep. 9, 14185.
Ballabio, A., Bonifacino, J.S., 2020. Lysosomes as dynamic regulators of cell and organismal homeostasis. Nat. Rev. Mol. Cell Biol. 21, 101–118.
Bartsch, U., et al., 2013. Apoptotic photoreceptor loss and altered expression of lysosomal proteins in the nclf mouse model of neuronal ceroid lipofuscinosis. Invest. Ophthalmol. Vis. Sci. 54, 6952–6959.
Bassal, M., et al., 2021. Rapid and progressive loss of multiple retinal cell types in Cathepsin D-deficient mice-an animal model of CLN10 disease. Cells. 10.
Benes, P., et al., 2008. Cathepsin D–many functions of one aspartic protease. Crit. Rev. Oncol. Hematol. 68, 12–28.
Bosch, M.E., Kielian, T., 2015. Neuroinflammatory paradigms in lysosomal storage diseases. Front. Neurosci. 9, 417.
Brandenstein, L., et al., 2016. Lysosomal dysfunction and impaired autophagy in a novel mouse model deficient for the lysosomal membrane protein Cln7. Hum. Mol. Genet. 25, 777–791.
Cao, Y., et al., 2006. Autophagy is disrupted in a knock-in mouse model of juvenile neuronal ceroid lipofuscinosis. J. Biol. Chem. 281, 20483–20493.
Carcel-Trullols, J., et al., 2015. Cell biology of the NCL proteins: what they do and don't do. Biochim. Biophys. Acta 1852, 2242–2255.
Dalkara, D., et al., 2009. Inner limiting membrane barriers to AAV-mediated retinal transduction from the vitreous. Mol. Ther. 17, 2096–2102.
D'Cruz, P.M., et al., 2000. Mutation of the receptor tyrosine kinase gene Mertk in the retinal dystrophic RCS rat. Hum. Mol. Genet. 9, 645–651.
Doccini, S., et al., 2016. Early infantile neuronal ceroid lipofuscinosis (CLN10 disease) associated with a novel mutation in CTSD. J. Neurol. 263, 1029–1032.
Flachsbarth, K., et al., 2014. Neural stem cell-based intraocular administration of ciliary neurotrophic factor attenuates the loss of axotomized ganglion cells in adult mice. Invest. Ophthalmol. Vis. Sci. 55, 7029–7039.
Fritchie, K., et al., 2009. Novel mutation and the first prenatal screening of cathepsin D deficiency (CLN10). Acta Neuropathol. 117, 201–208.
Fukumoto, Y., et al., 2010. Cost-effective gene transfection by DNA compaction at pH 4.0 using acidified, long shelf-life polyethylenimine. Cytotechnology. 62, 73–82.
Geraets, R.D., et al., 2016. Moving towards effective therapeutic strategies for neuronal ceroid Lipofuscinosis. Orphanet. J. Rare Dis. 11, 40.
Gonzalez-Cordero, A., et al., 2018. Assessment of AAV vector tropisms for mouse and human pluripotent stem cell-derived RPE and photoreceptor cells. Hum. Gene Ther. 29, 1124–1139.
Griffey, M., et al., 2005. AAV2-mediated ocular gene therapy for infantile neuronal ceroid lipofuscinosis. Mol. Ther. 12, 413–421.
Groh, J., et al., 2017. Fingolimod and teriflunomide attenuate neurodegeneration in mouse models of neuronal ceroid lipofuscinosis. Mol. Ther. 25, 1889–1899.
Hersheson, J., et al., 2014. Cathepsin D deficiency causes juvenile-onset ataxia and distinctive muscle pathology. Neurology. 83, 1873–1875.
Intartaglia, D., et al., 2021. Autophagy in the retinal pigment epithelium: a new vision and future challenges. FEBS J. https://doi.org/10.1111/febs.16018.
Jankowiak, W., et al., 2015. Sustained neural stem cell-based intraocular delivery of CNTF attenuates photoreceptor loss in the nclf mouse model of neuronal ceroid lipofuscinosis. PLoS One 10, e0127204.
Jankowiak, W., et al., 2016. Retinal degeneration in mice deficient in the lysosomal membrane protein CLN7. Invest. Ophthalmol. Vis. Sci. 57, 4989–4998.
Jeon, C.J., et al., 1998. The major cell populations of the mouse retina. J. Neurosci. 18, 8936–8946.
Jiang, M., et al., 2015. Microtubule motors transport phagosomes in the RPE, and lack of KLC1 leads to AMD-like pathogenesis. J. Cell Biol. 210, 595–611.
Johnson, T.B., et al., 2019. Therapeutic landscape for batten disease: current treatments and future prospects. Nat. Rev. Neurol. 15, 161–178.
Jung, G., et al., 2013. Genetically modified neural stem cells for a local and sustained delivery of neuroprotective factors to the dystrophic mouse retina. Stem Cells Transl. Med. 2, 1001–1010.
Karan, G., et al., 2005. Lipofuscin accumulation, abnormal electrophysiology, and photoreceptor degeneration in mutant ELOVL4 transgenic mice: a model for macular degeneration. Proc. Natl. Acad. Sci. U. S. A. 102, 4164–4169.
Kim, J.Y., et al., 2013. Noncanonical autophagy promotes the visual cycle. Cell. 154, 365–376.
Kleine Holthaus, S.M., et al., 2018. Prevention of photoreceptor cell loss in a Cln6(nclf) mouse model of batten disease requires CLN6 gene transfer to bipolar cells. Mol. Ther. 26, 1343–1353.
Klimczak, R.R., et al., 2009. A novel adeno-associated viral variant for efficient and selective intravitreal transduction of rat Muller cells. PLoS One 4, e7467.
Kohlschutter, A., et al., 2019. Current and emerging treatment strategies for neuronal ceroid lipofuscinoses. CNS Drugs. 33, 315–325.
Koike, M., et al., 2000. Cathepsin D deficiency induces lysosomal storage with ceroid lipofuscin in mouse CNS neurons. J. Neurosci. 20, 6898–6906.
Koike, M., et al., 2003. Involvement of two different cell death pathways in retinal atrophy of cathepsin D-deficient mice. Mol. Cell. Neurosci. 22, 146–161.
Koike, M., et al., 2005. Participation of autophagy in storage of lysosomes in neurons from mouse models of neuronal ceroid-lipofuscinoses (batten disease). Am. J. Pathol. 167, 1713–1728.
Kollmann, K., et al., 2013. Cell biology and function of neuronal ceroid lipofuscinosis-related proteins. Biochim. Biophys. Acta 1832, 1866–1881.
Lakkaraju, A., et al., 2020. The cell biology of the retinal pigment epithelium. Prog. Retin. Eye Res. 100846.
Laurent-Matha, V., et al., 2006. Processing of human cathepsin D is independent of its catalytic function and auto-activation: involvement of cathepsins L and B. J. Biochem. 139, 363–371.
Leinonen, H., et al., 2017. Retinal degeneration in a mouse model of CLN5 disease is associated with compromised autophagy. Sci. Rep. 7, 1597.

Marques, A.R.A., et al., 2020. Enzyme replacement therapy with recombinant pro-CTSD (cathepsin D) corrects defective proteolysis and autophagy in neuronal ceroid lipofuscinosis. Autophagy. 16, 811–825.
Meyer, S., et al., 2015. Congenital CLN disease in two siblings. Wien. Med. Wochenschr. 165, 210–213.
Mijanovic, O., et al., 2021. Cathepsin D-managing the delicate balance. Pharmaceutics. 13.
Mirza, M., et al., 2013. Progressive retinal degeneration and glial activation in the CLN6 (nclf) mouse model of neuronal ceroid lipofuscinosis: a beneficial effect of DHA and curcumin supplementation. PLoS One 8, e75963.
Mole, S.E., et al., 2019. Clinical challenges and future therapeutic approaches for neuronal ceroid lipofuscinosis. Lancet Neurol. 18, 107–116.
Mukherjee, A.B., et al., 2019. Emerging new roles of the lysosome and neuronal ceroid lipofuscinoses. Mol. Neurodegener. 14, 4.
Nakanishi, H., et al., 2001. Involvement of nitric oxide released from microglia-macrophages in pathological changes of cathepsin D-deficient mice. J. Neurosci. 21, 7526–7533.
Neverman, N.J., et al., 2015. Experimental therapies in the neuronal ceroid lipofuscinoses. Biochim. Biophys. Acta 1852, 2292–2300.
Palmer, D.N., et al., 2013. NCL disease mechanisms. Biochim. Biophys. Acta 1832, 1882–1893.
Radke, J., et al., 2015. Human NCL neuropathology. Biochim. Biophys. Acta 1852, 2262–2266.
Rakoczy, P.E., et al., 2002. Progressive age-related changes similar to age-related macular degeneration in a transgenic mouse model. Am. J. Pathol. 161, 1515–1524.
Regensburger, M., et al., 2020. Novel Biallelic CTSD gene variants cause late-onset Ataxia and retinitis Pigmentosa. Mov. Disord. 35, 1280–1282.
Saftig, P., et al., 1995. Mice deficient for the lysosomal proteinase cathepsin D exhibit progressive atrophy of the intestinal mucosa and profound destruction of lymphoid cells. EMBO J. 14, 3599–3608.
Sardiello, M., et al., 2009. A gene network regulating lysosomal biogenesis and function. Science. 325, 473–477.
Schaefers, J., et al., 2021. Presymptomatic treatment of classic late-infantile neuronal ceroid lipofuscinosis with cerliponase alfa. Orphanet. J. Rare Dis. 16, 221.
Schulz, A., et al., 2013. NCL diseases - clinical perspectives. Biochim. Biophys. Acta 1832, 1801–1806.
Schulz, A., et al., 2018. Study of intraventricular Cerliponase alfa for CLN2 disease. N. Engl. J. Med. 378, 1898–1907.
Settembre, C., Ballabio, A., 2014. Lysosomal adaptation: how the lysosome responds to external cues. Cold Spring Harb. Perspect. Biol. 6.
Shevtsova, Z., et al., 2010. CNS-expressed cathepsin D prevents lymphopenia in a murine model of congenital neuronal ceroid lipofuscinosis. Am. J. Pathol. 177, 271–279.
Siintola, E., et al., 2006. Cathepsin D deficiency underlies congenital human neuronal ceroid-lipofuscinosis. Brain. 129, 1438–1445.
Sleat, D.E., et al., 1999. Mutational analysis of the defective protease in classic late-infantile neuronal ceroid lipofuscinosis, a neurodegenerative lysosomal storage disorder. Am. J. Hum. Genet. 64, 1511–1523.
Sleat, D.E., et al., 2008. Residual levels of tripeptidyl-peptidase I activity dramatically ameliorate disease in late-infantile neuronal ceroid lipofuscinosis. Mol. Genet. Metab. 94, 222–233.
Sondhi, D., et al., 2020. Slowing late infantile batten disease by direct brain parenchymal administration of a rh.10 adeno-associated virus expressing CLN2. Sci. Transl. Med. 12.
Specchio, N., et al., 2021. Neuronal ceroid lipofuscinosis: potential for targeted therapy. Drugs. 81, 101–123.
Steinfeld, R., et al., 2006. Cathepsin D deficiency is associated with a human neurodegenerative disorder. Am. J. Hum. Genet. 78, 988–998.
Strauss, O., 2005. The retinal pigment epithelium in visual function. Physiol. Rev. 85, 845–881.
Tamaki, S.J., et al., 2009. Neuroprotection of host cells by human central nervous system stem cells in a mouse model of infantile neuronal ceroid lipofuscinosis. Cell Stem Cell 5, 310–319.
Thelen, M., et al., 2012. Disruption of the autophagy-lysosome pathway is involved in neuropathology of the nclf mouse model of neuronal ceroid lipofuscinosis. PLoS One 7, e35493.
Thottath, J., et al., 2019. A novel cathepsin D mutation in 2 siblings with late infantile neuronal ceroid lipofuscinosis. Neurol. Genet. 5, e302.
Tracy, C.J., et al., 2016. Intravitreal implantation of TPP1-transduced stem cells delays retinal degeneration in canine CLN2 neuronal ceroid lipofuscinosis. Exp. Eye Res. 152, 77–87.
Varvagiannis, K., et al., 2018. Congenital neuronal ceroid lipofuscinosis with a novel CTSD gene mutation: a rare cause of neonatal-onset neurodegenerative disorder. Neuropediatrics. 49, 150–153.
Vidoni, C., et al., 2016. The role of Cathepsin D in the pathogenesis of human neurodegenerative disorders. Med. Res. Rev. 36, 845–870.
von Eisenhart-Rothe, P., et al., 2018. Failure of autophagy-lysosomal pathways in rod photoreceptors causes the early retinal degeneration phenotype observed in Cln6nclf mice. Invest. Ophthalmol. Vis. Sci. 59, 5082–5097.
Wavre-Shapton, S.T., et al., 2014. Phagosome maturation during endosome interaction revealed by partial rhodopsin processing in retinal pigment epithelium. J. Cell Sci. 127, 3852–3861.
Wavre-Shapton, S.T., et al., 2015. Photoreceptor phagosome processing defects and disturbed autophagy in retinal pigment epithelium of Cln3Deltaex1-6 mice modelling juvenile neuronal ceroid lipofuscinosis (batten disease). Hum. Mol. Genet. 24, 7060–7074.
Whiting, R.E.H., et al., 2020a. Intravitreal enzyme replacement preserves retinal structure and function in canine CLN2 neuronal ceroid lipofuscinosis. Exp. Eye Res. 197, 108130.
Whiting, R.E.H., et al., 2020b. Intravitreal enzyme replacement inhibits progression of retinal degeneration in canine CLN2 neuronal ceroid lipofuscinosis. Exp. Eye Res. 198, 108135.
Yadati, T., et al., 2020. The ins and outs of Cathepsins: physiological function and role in disease management. Cells. 9.
Yamasaki, R., et al., 2007. Involvement of lysosomal storage-induced p38 MAP kinase activation in the overproduction of nitric oxide by microglia in cathepsin D-deficient mice. Mol. Cell. Neurosci. 35, 573–584.
Zaidi, N., et al., 2008. Cathepsin D: a cellular roadmap. Biochem. Biophys. Res. Commun. 376, 5–9.
Zhang, D., et al., 2002. A model for a blinding eye disease of the aged. Biogerontology. 3, 61–66.